THESIS FOR THE DEGREE OF LICENTIATE OF ENGINEERING

Advancing Moderate to Severe Neck Injury Prediction in Motor Vehicle Crashes

Development of a Cervical Spine Model and a Ligament Injury Risk Function

YASH NIRANJAN POOJARY



Department of Mechanical Engineering
CHALMERS UNIVERSITY OF TECHNOLOGY

Gothenburg, Sweden 2026

Advancing Moderate to Severe Neck Injury Prediction in Motor Vehicle Crashes
Development of a Cervical Spine Model and a Ligament Injury Risk Function

YASH NIRANJAN POOJARY

© YASH NIRANJAN POOJARY, 2026.

Thesis for Licentiate of Engineering

Department of Mechanical Engineering
Chalmers University of Technology
SE-412 96 Gothenburg
Sweden
Telephone + 46 (0)31-772 1000

Cover:
Neutral zone (NZ) of the cervical spine, expressed as a percentage of the range of motion (RoM), across spinal levels (C0–C1 to C6–C7) and motions (flexion, extension, lateral bending and axial rotation). Values were compiled from in vitro studies (Panjabi et al., 1988, 1991, 1994, 2001; Oda et al., 1992; Wen et al., 1993; Richter et al., 2000; Hartman et al., 2016; Jonas et al., 2020), tested at moments of 1–4 Nm, and interpolated between levels and motions. The darker line marks the average NZ of 47% of the RoM.

Printed by Chalmers Reproservice
Gothenburg, Sweden 2026

The only thing we're allowed to do is to believe that we won't regret the choice we made.

— Levi Ackerman

ABSTRACT

Moderate to severe cervical spine injuries in motor vehicle crashes are not common, but if they occur, they present an acute threat to life or can have severe neurological consequences leads to long-term disability. The most frequent specific injuries, compression fractures and dislocations in the lower cervical spine, have not declined in incidence despite advances in vehicle safety. Occupants of novel automated vehicles are expected to adopt a wider range of seating postures, such as reclined seating, which is associated with a higher likelihood of neck injury. Crash test dummies assess neck injury risk from global metrics, are limited to specific loading directions and postures, and cannot indicate which cervical structure is at risk. Finite Element Human Body Models (HBMs) can predict injury in the individual structures and can be morphed to represent a diverse occupant population. However, neck injury risk in HBMs is still assessed mainly with global criteria, and local (individual-structure) criteria are often deterministic thresholds that do not account for variability between individuals. To predict local injury risk across the occupant population, HBMs therefore need a cervical spine model that reproduces the spinal response and its variability, and local injury risk functions that account for variability between individuals.

In this thesis, a ligamentous FE model of the lower cervical spine and a ligament injury risk function (IRF) for the cervical spine were developed. The model, representing an average male based on aggregated literature data, was calibrated by adjusting the unstretched ligament lengths against stepwise-reduction tests to account for the difference between in vitro and in situ ligament length. The model was then validated with respect to independent range of motion and instantaneous centre of rotation data and was within the experimental corridors. Variability in vertebral geometry contributed more to the spread in segmental response observed in experiments than variability in ligament material properties. This development was followed by the construction of ligament IRFs from tensile tests on 261 ligaments from 16 Post-Mortem Human Subjects (PMHS), using a hierarchical Bayesian survival model that accounts for several tested ligaments being obtained from each PMHS and for the dependence between the left and right capsular ligaments of the same segment. Ligament type and initial length were the main predictors of failure elongation, and the effect of initial length differed between ligament types, being largest for the posterior longitudinal ligament and ligamentum flavum and smallest for the anterior longitudinal ligament. The variation between PMHS was small compared to variation within the tests. Within the tested cohort, age, sex and strain rate did not improve the predictive performance. The quality of the IRFs was deemed good for all ligaments, risk levels and initial lengths.

The model and the IRFs developed in this thesis provide a step towards advancing the prediction of moderate to severe neck injuries in HBMs, with a focus on ligament failure. The model showed that population-level HBMs should account for variability in both vertebral geometry and ligament material properties, with vertebral geometry having the larger influence on the segmental response. The IRFs, in turn, allow the risk of ligament failure to be estimated for each ligament type and initial length, accounting for the variability between individuals. The next step is to combine the model and the IRFs, which requires a consistent definition of ligament elongation and a description of how the in situ ligament length changes with posture. Reconstructions of whole-body PMHS tests using HBMs can then evaluate the injury prediction in different seating postures. Combining the failure risks of the ligaments of a segment would finally allow segmental injuries such as dislocations to be predicted.

Keywords: Cervical spine, Human body model, Ligament slack, Population variability, Injury risk function, Range of motion, Instantaneous centre of rotation, Bayesian survival analysis

LIST OF APPENDED PAPERS

Paper A	**Poojary, Y. N.**, Östh, J., Davidsson, J., John, J., Iraeus, J. Influence of Population Variability in Ligament Material and Vertebrae Geometry on Cervical Spine Responses Published and presented at: *Proceedings of IRCOBI Conference 2026, Munich, Germany*
Paper B	**Poojary, Y. N.**, Östh, J., Davidsson, J., John, J., Iraeus, J. Development of a Ligament Level Injury Risk Function for the Cervical Spine *Draft Manuscript*

PREFACE

The research presented in this licentiate thesis was conducted at the Division of Vehicle Safety, Department of Mechanical Engineering, Chalmers University of Technology in Gothenburg, Sweden, between April 2024 and November 2026, under the supervision of Johan Davidsson, Johan Iraeus, Jonas Östh and Jobin John, and examined by Mats Svensson.

Acknowledgements

To my four supervisors, Johan, Johan, Jonas and Jobin… thank you. Each brought a different voice, and together you kept this work in tune (and fun). Thank you for your trust, patience and encouragement, for always making time for my questions and reading my drafts (often at short notice), for all the advice on writing and presentations, and for bearing with me (hopefully for a few more years). I couldn't have asked for a better set.

A big thanks to my fellow PhD students, Ali, Linus, Chiara, Oscar, Shwetha and Emmi, and to Shinya and Oscar, for the discussions and the laughs (over fika and lunch) that make the office fun, even when the simulations refuse to cooperate. Thank you also to Alexandros, Emma and Erik… seeing you go through your PhDs is a big part of why I wanted to start mine.

Finally, to my mom, dad and Tanish… none of this would have been possible without your patience and belief in me.

Yash

November 2026

Funding and Project Partners

The work was carried out at the Division of Vehicle Safety, Chalmers and at the SAFER – The Vehicle and Traffic Safety Centre at Chalmers. The work was funded by Vinnova and the industry partners, Autoliv Research, Folksam, and Volvo Car Corporation, through the Traffic-safe Automation sub-program within the Strategic Vehicle Research and Innovation program (FFI, Award Number: 2023-02612). Simulations were performed on resources provided by the National Academic Infrastructure for Supercomputing in Sweden (NAISS).

Declaration of AI use

A generative AI model (Claude Opus 5.5, Anthropic, 2026) was used to improve the grammar, clarity and flow of the text, to suggest alternative phrasings and structures for paragraphs written by the author, and to generate Python scripts and schematic illustrations for selected figures, which are marked in their captions. The tool was not used to generate research data, results or interpretations, nor as a source of scientific information. All suggested text was reviewed, edited and verified against the original literature by the author, who takes full responsibility for the content of the thesis.

ABBREVIATIONS

AFT	Accelerated Failure Time
AIS	Abbreviated Injury Scale
AIS2+	Injuries Of AIS2 Or Higher (Moderate to Severe)
ALL	Anterior Longitudinal Ligament
ATD	Anthropometric Test Device
BioRID	Biofidelic Rear Impact Dummy
CIREN	Crash Injury Research and Engineering Network
CISS	Crash Investigation Sampling System
CL	Capsular Ligament
C0	Occiput (base of the skull)
C1-C7	First to seventh cervical vertebrae
CrI	Credibility Interval
DAG	Directed Acyclic Graph
ELPD-LOO	Expected Log Pointwise Predictive Density, Estimated by Leave-One-Out Cross-Validation
FE	Finite Element
FSU	Functional Spinal Unit
GHBMC	Global Human Body Models Consortium
HBM	Human Body Model
ICR	Instantaneous Centre of Rotation
IRF	Injury Risk Function
ISL	Interspinous Ligament
IVD	Intervertebral Disc
LCS	Ligamentous Cervical Spine
LF	Ligamentum Flavum
MCMC	Markov Chain Monte Carlo
MVC	Motor Vehicle Crash
NASS	National Automotive Sampling System
NIC	Neck Injury Criterion
N_{ij}	Neck Injury Criterion Combining Axial Force and Flexion–Extension Moment
N_{km}	Neck Injury Criterion Combining Shear Force and Flexion–Extension Moment
NSCISC	National Spinal Cord Injury Statistical Centre
NZ	Neutral Zone
PLL	Posterior Longitudinal Ligament
PMHS	Post-Mortem Human Subject
RoM	Range Of Motion
SD / SE	Standard Deviation / Standard Error
SHBM	SAFER Human Body Model
THOR	Test Device for Human Occupant Restraint
THUMS	Total Human Model for Safety

TABLE OF CONTENTS

ABSTRACT i

LIST OF APPENDED PAPERS iii

PREFACE iv
- Acknowledgements iv
- Funding and project partners v
- Declaration of AI use v

ABBREVIATIONS vi

TABLE OF CONTENTS vii

INTRODUCTION 1
- Cervical Spine Injuries in Motor Vehicle Crashes 1
- Cervical Spine Injuries in Belted Occupants 2
- Injury Assessment in Crash Safety Using Occupant Surrogates 2

AIM AND OBJECTIVES 4

BACKGROUND 5
- Cervical Spine Anatomy 5
- Kinematics and coupled spinal motion 8
- Neutral zone 9
- Injury mechanisms and classification 10
- Finite Element Neck Models 11
- Injury Criteria 12
- Survival Modelling for Injury Risk Functions 13
- Bayesian Fit of Survival Models 14

SUMMARY OF PAPER A 15
- Methods 15
- Results and discussion 16

SUMMARY OF PAPER B 17
- Methods 17
- Results and discussion 17

DISCUSSION 19
- Ligament Initial Length 19
- Injury Risk Function 20
- Further Applications 20
- Beyond the Average Male 21

CONCLUSIONS 22

FUTURE WORK 24

REFERENCES 26

CHAPTER 1

INTRODUCTION

In Motor Vehicle Crashes (MVCs), the cervical spine may be exposed to a wide range of loading conditions and severities. Potential injuries range from minor soft-tissue injuries, through injuries to ligaments and facet joints, to fractures and dislocations of the upper (skull to second cervical vertebra, C0–C2) or lower (C3 to first thoracic vertebra, T1) cervical spine, which can also cause injury to the spinal cord. The most common cervical spine injuries are minor soft-tissue injuries, often referred to as whiplash-associated disorders, which may nonetheless lead to long-term impairment. Moderate and more severe injuries of Abbreviated Injury Scale (AIS) level 2 or higher (AIS2+) are less common, but can cause long-term disability and severe neurological consequences, particularly when the spinal cord is involved (Waseem *et al.*, 2025).

Cervical Spine Injuries in Motor Vehicle Crashes

In the United States (US), crash-related cervical spine injuries seen in hospitals are estimated at about 869,000 per year. Most are minor (AIS1) sprain injuries, and only about 3% are AIS2+, but these include about 23,500 fractures and 1,500 dislocations (Freeman and Leith, 2020). The more severe (AIS2+) cervical spine injuries can also involve the spinal cord. Of the over 18,000 new traumatic spinal cord injuries in the US each year, about 37% are caused by MVCs (NSCISC, 2025). In earlier clinical studies, MVCs were the single largest cause of cervical spine injury, accounting for 52–68% of cases, and injuries between C5 and C7 dominated in adults under 50 years (Myers and Winkelstein, 1995).

Most epidemiological data on cervical spine injuries in MVCs come from US national crash databases. In data from the National Automotive Sampling System (NASS) for 1979–1986, the cervical spine accounted for two thirds of all AIS3+ spine injuries (Yoganandan *et al.*, 1989). Al-Salehi *et al.* (2024) compared NASS (2005–2015) with its replacement, the Crash Investigation Sampling System (CISS, 2017–2022). In both, vertebral injuries (fractures or dislocations without spinal cord injury) made up most cervical spine injuries (84% in NASS and 91% in CISS), and cervical fractures were five to six times more likely in rollovers than in other crash scenarios, a risk that remained high in the more recent fleet. In German crash data, 0.24% of front-seat occupants in police-reported collisions sustained a cervical fracture, most often in multiple collisions, followed by side and frontal collisions (Müller *et al.*, 2014). In Sweden, fracture register and crash data for 2014–2016 showed that 69% of all vertebral fractures in MVCs occurred in car occupants (Meredith *et al.*, 2020). Among all adults treated for lower cervical spine fractures in the Swedish Fracture Register between 2013 and 2021, high-energy trauma, including MVCs, accounted for 41% of the surgically and 31% of the non-surgically treated cases, and the C5–C7 levels were the most affected (Buwaider *et al.*, 2024).

Crash data show frequency and crash scenarios resulting in cervical spine injuries, but they give limited detail on the injury type and level, and NASS has been shown to underestimate crash-related cervical spine injuries by about 84% (Freeman and Leith, 2020). Clinical data classify the injuries in more detail. Among MVC patients treated at a US hospital, the C5 and C6 vertebrae were the most injured, anterior wedge fractures were the most common fracture type, and dislocations occurred mainly between the fourth and seventh cervical vertebrae (Yoganandan *et al.*, 1989). Among cervical fractures from all causes (MVC, falls, etc..), facet fractures, often leading to instability, were the most frequent lower cervical spine fracture (Utheim *et al.*, 2022).

Cervical Spine Injuries in Belted Occupants

The data summarized above include both belted and unbelted occupants. Although seatbelts reduce the risk of cervical spine injury, they do not eliminate it (Yoganandan *et al.*, 1989, Claytor *et al.*, 2004). In the early NASS data, only 20% of the occupants were belted, and belt use markedly reduced the incidence of AIS3+ cervical injuries. In frontal crashes in NASS for 1995–2001, seatbelt use reduced the risk of AIS2+ cervical spine injury, yet over a third of the occupants who sustained such an injury wore only a seatbelt (Claytor *et al.*, 2004). For front-seat occupants in NASS for 2000–2015, excluding rollovers and multiple impacts, frontal crashes led to the highest incidence of cervical fractures, and drivers were at greater risk than front-seat passengers (Pipkorn *et al.*, 2020). In CISS and the Crash Injury Research and Engineering Network (CIREN) database, a third of AIS3+ spine injuries in front-seat occupants occurred in the cervical spine, almost half of them in frontal impacts (Rudd and Parenteau, 2023).

For AIS2+ cervical spine injuries, dislocations of the lower cervical spine are of particular concern. Cervical spine dislocations are associated with high neurological morbidity and mortality, and lower cervical spine dislocations account for up to 75% of them (Foroutan *et al.*, 2024). In US national hospital data, about 1,500 MVC related cervical spine dislocations are seen each year (Freeman and Leith, 2020). In a cohort of 226 patients with sub-axial facet subluxation or dislocation at an Australian trauma centre, MVC were the most common cause (59%), the C6–C7 level was most often involved, and a third of the patients had a spinal cord injury (Quarrington *et al.*, 2018). Among severely injured occupants in CIREN, spinal cord injury occurred in 62% of sub-axial dislocations (Foroutan *et al.*, 2024), compared with 11% of all occupants with cervical spine injury in NASS (Al-Salehi *et al.*, 2024). The Swedish Fracture Register shows the same pattern, surgically treated sub-axial injuries were mainly translation (dislocation-type) injuries, with spinal cord injury in 24% of patients, whereas non-surgically treated injuries were mainly compression fractures, with spinal cord injury in 1% (Buwaider *et al.*, 2024). About half of the occupants with cervical spine dislocations in NASS and CISS were restrained with a three-point belt, and the dislocations resulted mainly from frontal (41%) and near-side (28%) crashes, with only 13% from pure rollovers (Foroutan *et al.*, 2024). Cervical fractures, in contrast, are most frequent in rollovers (Al-Salehi *et al.*, 2024, Dutschke *et al.*, 2023).

While the seatbelt restrains the torso, the head is free to move, and the cervical spine can be loaded by the inertia of the head alone in a crash. Huelke *et al.* (1993) reviewed cervical fractures and dislocations in belted occupants without head impact, including lower cervical dislocations at C5-C6 and C6-C7. They attributed these injuries to forward flexion of the neck, with or without distraction, but noted that they are rare. Among severely injured occupants in CIREN, lower cervical spine dislocations occurred most frequently at C6-C7 and C5-C6 and were mainly associated with head or face impact with the upper vehicle interior (52%), seatbelt restraint of the torso (19%) and the airbag (11%), with neck loading typically involving flexion or extension (Foroutan *et al.*, 2024). In a single-centre cohort of belted drivers with airbag deployment, all cervical spine injuries were hyperextension injuries, and half of them were dislocations (Inamasu and Kato, 2018). These studies suggest that dislocations in belted occupants may arise from more than one loading mode. Their mechanisms nevertheless remain unclear, as the evidence comes from case reviews, small cohorts and databases biased toward severe crashes.

Across these mechanisms, a dislocation requires several of the ligaments connecting two adjacent vertebrae to fail, so that one vertebra can translate relative to the other. Predicting cervical spine dislocations in restrained occupants therefore requires knowing at what loading the ligaments fail.

Injury Assessment in Crash Safety Using Occupant Surrogates

In the development of car occupant protection systems, Anthropometric Test Devices (ATDs) are used to assess injury risk from global deflections, forces, moments and accelerations, using criteria developed for specific ATDs and loading directions. However, ATDs have several limitations, such as a directionally dependent response, a lack of muscle responses and a limited number of sizes (Yoganandan *et al.*, 2014). For neck injury assessment, the BioRID II (Davidsson, 1999), used to assess rear-impact injuries, is limited to the fore–aft kinematics of upright occupants and represents an average male. A female counterpart, the

EvaRID, was first developed as a finite element model (Carlsson *et al.*, 2012), and a physical version has only recently been evaluated (Isopi *et al.*, 2026).

Finite Element (FE) Human Body Models (HBMs), such as the Global Human Body Models Consortium (GHBMC) model (Gayzik *et al.*, 2011), Total Human Model for Safety (THUMS) (Shigeta *et al.*, 2009), VIVA+ (John *et al.*, 2022) and the SAFER Human Body Model (SHBM) (Iraeus *et al.*, 2024), offer an alternative by representing the human anatomy in detail. They can be used for detailed virtual simulations of the human anatomy and can be used to study how physical forces, impacts, or loads affect the body. They are omnidirectional by design, can be positioned in different postures, and can include active muscle responses (Östh *et al.*, 2025), which are central to load sharing in the neck. For HBMs, localized injury risk can be predicted, and the models can be morphed to account for differences in age, sex, stature and weight (Larsson *et al.*, 2024), allowing occupant protection to be assessed for occupants of both sex and of different sizes. This makes HBMs suited for analysing crash scenarios beyond the standard sizes and upright seated occupants, for which the limitations of ATDs become more pronounced. In addition, occupants of automated vehicles may adopt a wider range of seating postures, such as reclined or turned seating, which have been associated with a higher likelihood of neck injury (McMurry *et al.*, 2018, Schaefer *et al.*, 2021, Leledakis *et al.*, 2021).

To predict cervical spine injuries for occupants, in non-standard postures and in any loading direction, an HBM requires a cervical spine model that reproduces the response of the spine and its variability across the population, together with local injury criteria that relate the predicted response to a risk of injury.

CHAPTER 2

AIM AND OBJECTIVES

The aim of this PhD project is to advance the prediction of moderate and more severe cervical spine (AIS2+) injuries in MVCs, accounting for individual variability, so that injury risk can be assessed across occupants, crash scenarios and seating postures beyond what current tools allow. The models and injury risk functions developed are intended to be incorporated into whole-body HBMs. To fulfil this aim, five objectives have been defined. This licentiate thesis addresses the first two, as a step towards the main aim:

- Develop, calibrate and validate a finite element model of the average male lower cervical spine, and evaluate how population variability in vertebral geometry and ligament material affects its response (Paper A).
- Develop an injury risk function for the cervical spine ligaments, for injury prediction with human body models (Paper B).

The following three objectives will be the focus of the remainder of the PhD project and are not addressed in this licentiate thesis:

- Extend the new model to the upper cervical spine and validate the full cervical spine under dynamic and injurious loading.
- Extend the ligament injury risk function to predict cervical spine injury, accounting for uncertainty and population variability.
- Incorporate the cervical spine model and injury risk function in a whole-body HBM and validate the predictions in whole-body simulations of moderate to high severity crashes.

CHAPTER 3

BACKGROUND

Cervical Spine Anatomy

The human spine normally includes seven cervical, twelve thoracic and five lumbar vertebrae, together with the sacrum and the coccyx. The vertebrae are connected by intervertebral discs, ligaments and muscles. The cervical spine supports the head, protects the spinal cord and vertebral arteries, and allows a wide range of head motion. The cervical spine extends from the base of the skull to the thorax.

Vertebrae

The seven cervical vertebrae fall into two groups, the typical vertebrae of the lower cervical spine and the atypical atlas (C1) and axis (C2) of the upper cervical spine. The lower cervical vertebrae share a common structure (Figure 1), with an anterior vertebral body and a posterior vertebral arch. The anterior vertebral body, trabecular bone within a thin cortical shell, carries most of the compressive load. The arch comprises the laminae, the articular facets, which form the facet joints with the adjacent vertebrae, and the transverse and spinous processes, which serve as attachments for ligaments and muscles. Together, the body and arch enclose the vertebral foramen, which contains, and protects, the spinal cord. Compared with a lumbar vertebra, the cervical vertebra has a smaller, oval body with raised lateral margins called the uncinate processes, a relatively larger vertebral foramen, transverse foramina for the vertebral arteries, and a bifid spinous process.

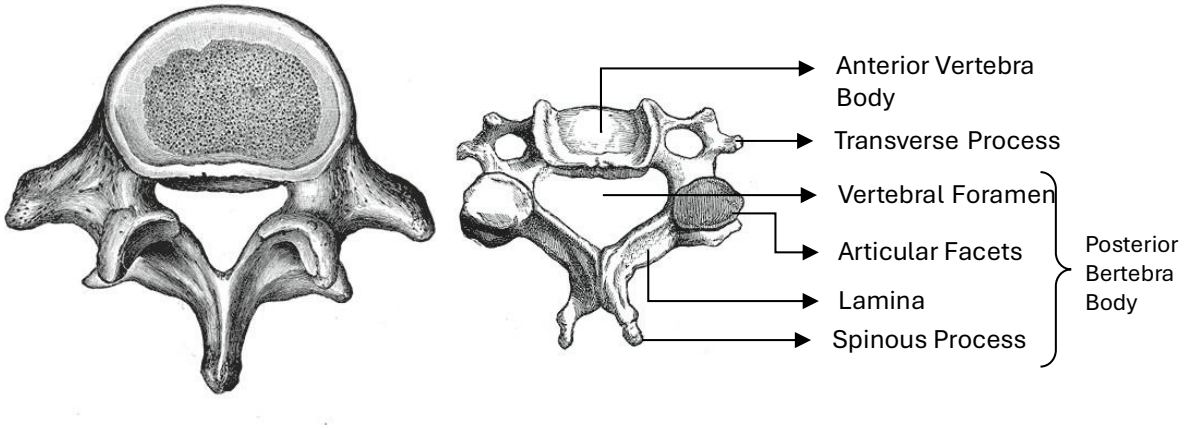


Figure 1 Superior view of a lumbar vertebra (left) and a cervical vertebra (right). *Adapted from (Gray, 1918)*

The atlas (C1) and axis (C2) have a different structure from the typical vertebrae (Figure 2). The atlas has no vertebral body. It is a ring formed by an anterior and a posterior arch, with large superior articular facets that articulate with the occipital condyles to form the atlantooccipital joint. The axis has a vertical projection, the dens, which articulates with the anterior arch of the atlas to form the atlantoaxial joint. Like the typical vertebrae, both carry transverse processes, and the axis has a large spinous process.

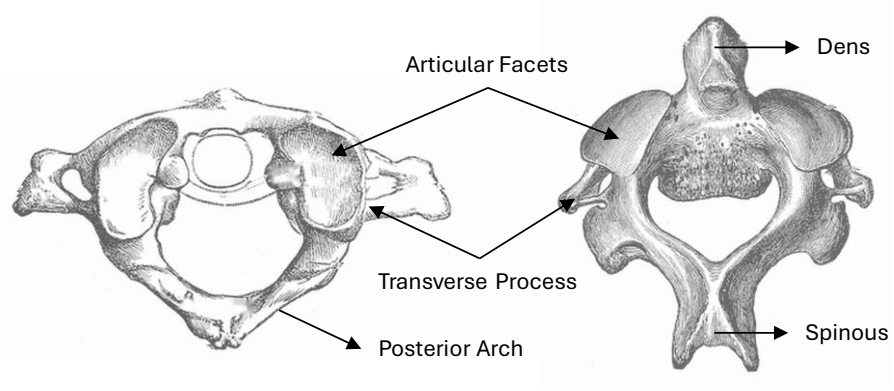


Figure 2 Superior view of the atlas, C1 (left), and posterosuperior view of the axis, C2 (right). *Adapted from (Gray, 1918)*

Intervertebral Discs and Endplates

An Intervertebral Disc (IVD) connects adjacent vertebral bodies from C2–C3 and downward, there are none at C0–C1 and C1–C2. Each disc consists of a centrally located nucleus pulposus with a surrounding annulus fibrosus (Figure 3a, b) and is separated from the vertebral body by the endplate, which consists of a cartilaginous layer and a bony layer (Figure 3c). The nucleus is a gel of mainly water and proteoglycans. The annulus is made of concentric lamellae of collagen fibres, with the fibre direction alternating between adjacent lamellae. Unlike the lumbar disc, the cervical annulus is thick and crescent-shaped anteriorly and thin posteriorly (Mercer and Bogduk, 1999, Tonetti *et al.*, 2005). Anteriorly, it consists of concentric lamellae in which the collagen fibres run obliquely, with the fibre direction alternating between adjacent lamellae. Posteriorly, the annulus is reduced to a thin layer of mainly vertical fibres, covered by the posterior longitudinal ligament (Mercer and Bogduk, 1999). In the cervical disc, the boundary between nucleus and annulus is less distinct than in the lumbar disc and fades further with age (Fontes *et al.*, 2015).

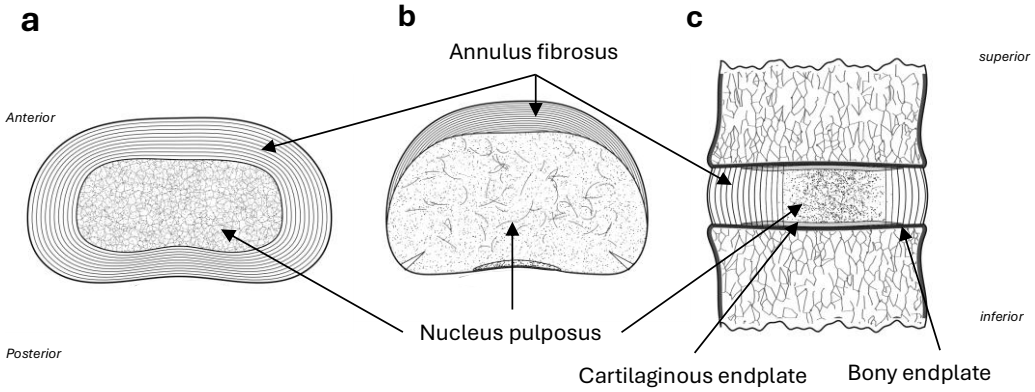


Figure 3 Intervertebral disc. Axial view of (a) a lumbar and (b) a cervical disc, showing the nucleus pulposus and annulus fibrosus. (c) Schematic section through a cervical segment, showing the cartilaginous and bony endplates separating the disc from the vertebral bodies. Image created with the assistance of generative AI (Claude, Anthropic)

Facet Joints

The facet joints are synovial joints between the articular processes of adjacent vertebrae, and their geometry guides segmental motion. Each joint is enclosed by a capsular ligament, lined with a synovial membrane and lubricated by synovial fluid. The facets are ovoid, with slightly convex superior and slightly concave inferior surfaces, and their cartilage is about 1–1.4 mm thick and thickest centrally (Womack *et al.*, 2008). Adult facets are inclined roughly 45° to the transverse plane, increasing caudally from about 35° at C2, and about 70°–85° to the sagittal plane from C3 to C7 (Pal *et al.*, 2001, Panjabi *et al.*, 1993).

Ligaments

The ligaments connect adjacent vertebrae and together with the discs and facet joints, determine the range of segmental motion. In the lower cervical spine, five ligaments connect each pair of vertebrae (Figure 4c, d). The anterior and posterior longitudinal ligaments (ALL, PLL) run along the front and back of the vertebral bodies and discs. The ligamentum flavum (LF) connects adjacent laminae, and its high elastin content gives it rubber-like properties. The capsular ligaments (CL) enclose the facet joints, and the interspinous ligament (ISL) connects the spinous processes.

The upper cervical spine has no discs, and its stability relies on a separate set of ligaments (Figure 4a, b). The transverse ligament holds the dens against the anterior arch of the atlas and, together with its vertical bands, forms the cruciform ligament. This creates the central pivot of the atlantoaxial joint. The alar ligaments connect the sides of the dens to the occipital condyles and limit axial rotation, while the apical ligament connects the tip of the dens to the foramen magnum of the skull. Posteriorly, the tectorial membrane continues the PLL from the body of C2 to the occiput. The ALL and LF continue cranially as the anterior and posterior atlantooccipital and atlantoaxial membranes (AAOM, PAOM, AAAM, PAAM), spanning the atlantooccipital joints, mainly allowing flexion-extension motions.

Two further structures are often listed among the cervical ligaments but are not considered here. The intertransverse ligaments are reduced to a few scattered fibres in the cervical spine (Gray, 1918). The supraspinous ligament connects the tips of the spinous processes from the thoracic spine downwards, and in the neck, it is often described as continuing as the ligamentum nuchae. The ligamentum nuchae spans from the external occipital protuberance to the spinous process of C7, but consists of a dorsal raphe formed by the tendons of the posterior neck muscles and a midline fascial septum, rather than a ligament connecting adjacent vertebrae (Mercer and Bogduk, 2003).

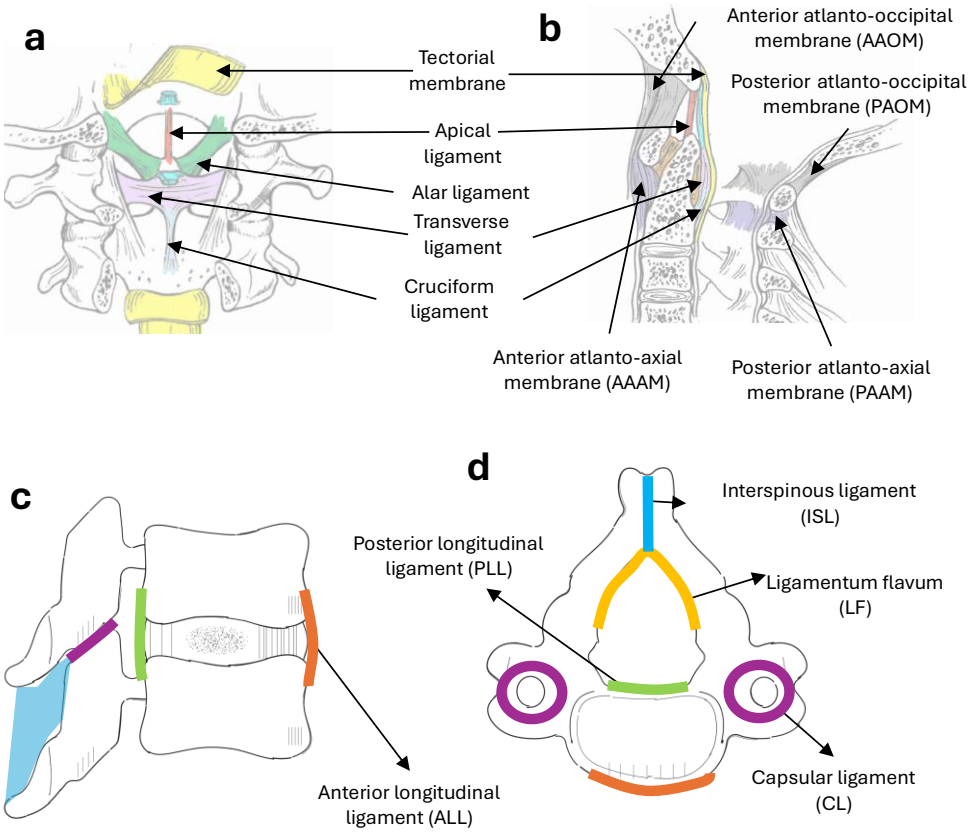


Figure 4 Ligaments of the cervical spine. Upper cervical spine: (a) posterior view with the vertebral canal opened and (b) mid-sagittal view. Lower cervical spine: (c) lateral view and (d) superior view. Panel (a) and (b) Adapted from (Gray, 1918) panel c and d created with the assistance of generative AI (Claude, Anthropic)

Kinematics and Coupled Spinal Motion

Motion of a cervical spinal segment is normally (and in this thesis) described in a local coordinate system with the x-axis pointing anteriorly, the y-axis to the left and the z-axis superiorly. Rotations about these axes define the three primary motions: flexion-extension about the y-axis (Figure 5a), lateral bending about the x-axis (Figure 5b) and axial rotation about the z-axis (Figure 5c). Forces along the same axes act as antero-posterior shear (x), lateral shear (y) and compression or tension (z). Each segment therefore has six degrees of freedom: three rotations and three translations.

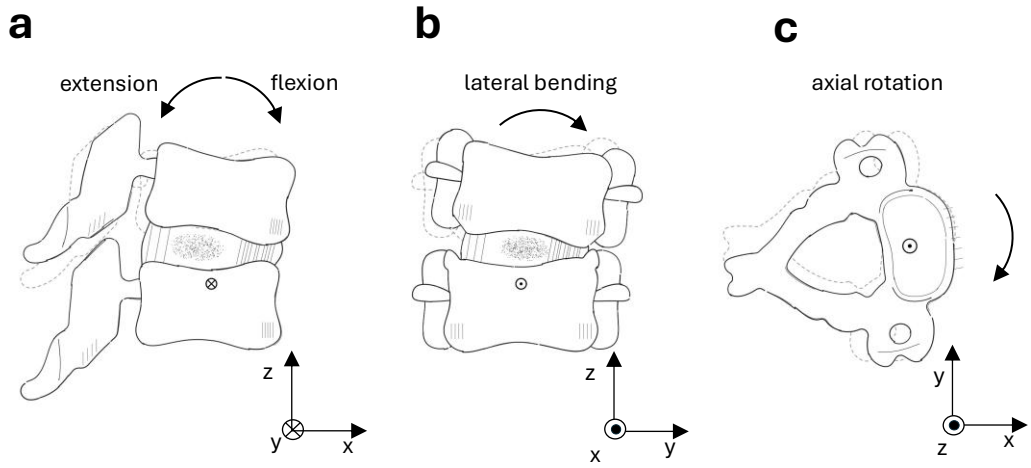


Figure 5 Primary motions of a cervical spinal segment, with the neutral position shown dashed and the displaced position solid (a) flexion-extension about the y-axis (side view), (b) lateral bending about the x-axis (front view), and (c) axial rotation about the z-axis (top view). Image created with the assistance of generative AI (Claude, Anthropic)

The Range of Motion (RoM) of a segment is the rotation reached in a primary motion under a specified load. In vitro, it is typically measured by applying a pure moment of a given magnitude to the upper vertebra and recording its rotation relative to the lower vertebra, and it is reported separately. Because RoM depends on the applied moment, values are only comparable between studies at the same load and load speed. A primary motion is often accompanied by motion in other degrees of freedom, termed coupled motion.

The upper and lower cervical spine contribute differently to these motions in the overall cervical spine (Kapandji, 1974, Bogduk and Mercer, 2000). The upper cervical spine, formed by the occiput, atlas and axis (C0–C2), provides most of the axial rotation of the head (Panjabi *et al.*, 1988). Its atlantooccipital joints have spherical articular surfaces and allow mainly flexion-extension, with only a few degrees of lateral bending and little axial rotation. The atlantoaxial joint combines a central pivot with two lateral facet joints. In the pivot, the dens rotate within a ring formed by the anterior arch of the atlas and the transverse ligament. Because the superior facets of the axis are convex, the atlas descends by 2–3 mm as it rotates, so axial rotation at C1–C2 follows a helical path rather than a pure rotation (Kapandji, 1974). The transverse ligament keeps the dens in contact with the atlas during flexion-extension, and the alar ligaments limit axial rotation.

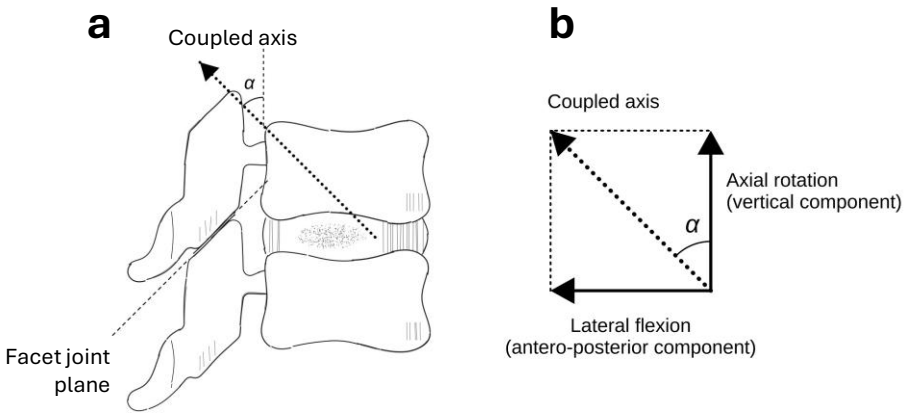


Figure 6 Coupled motion of the lower cervical spine. (a) Lateral view of two adjacent vertebrae: sliding in the oblique facet joint plane produces rotation about an axis perpendicular to it, inclined at α to the vertical. (b) This rotation combines axial rotation and lateral flexion, in proportions set by α. Image created with generative AI (Claude, Anthropic) based on Kapandji (1974), Figs. 47 and 53.

The lower segment (C2–T1), lateral bending and axial rotation are coupled (Kapandji, 1974, Panjabi *et al.*, 2001). In flexion-extension, for each vertebrae pair, the superior vertebra both rotates and translates relative to the inferior one (Bogduk and Mercer, 2000). The disc is compressed on one side and tensed on the other, and the facet joints open. Extension is limited by the ALL and by contact between the posterior bony elements, whereas flexion is limited only by the posterior ligaments (PLL, CL, LF and ISL), which therefore fail first in hyperflexion. Over the whole neck, the ligamentum nuchae also resists flexion. In lateral bending and axial rotation, the facet joints determine the coupling. The facets lie in an oblique plane, so sliding between them can only produce rotation about an axis perpendicular to that plane, inclined at an angle α to the vertical (Figure 6a). This rotation combines axial rotation and lateral bending in proportions set by α (Figure 6b). At C2–C3 the axis is inclined about 45°, giving roughly equal rotation and lateral bending, whereas at C7–T1 it is almost vertical, giving almost pure rotation (Kapandji, 1974). As a result, the lower cervical spine cannot produce pure lateral bending or pure axial rotation on its own. For example, tilting the head to the right also rotates it to the right, because the inclined facet joints of the lower cervical spine make lateral bending and axial rotation occur together. The upper cervical spine counteracts this rotation, allowing the head to tilt while still facing forward (Kapandji, 1974).

Neutral Zone

Panjabi (1992) defined the Neutral Zone (NZ) as "*the part of the range of physiological intervertebral motion, measured from the neutral position, within which the spinal motion is produced with a minimal internal resistance*". Physically, the NZ is the laxity of a spinal segment around the neutral posture, where the passive structures (ligament, disc and facets) offer little resistance, resulting in segmental motion under small loads. Others have described it differently, (Wilke *et al.*, 1998) described the NZ in the light of the hysteresis shown in cycled loading, where the specimen returns along a different path during unloading than during loading, while (Crawford *et al.*, 1998) described it as a creep-like behaviour, where the specimen, once loaded and released, does not return to its original position. The NZ increases with injury and was found to be more sensitive than RoM (Oxland and Panjabi, 1992). It has therefore been proposed as an indicator of spinal instability (Panjabi, 1992).

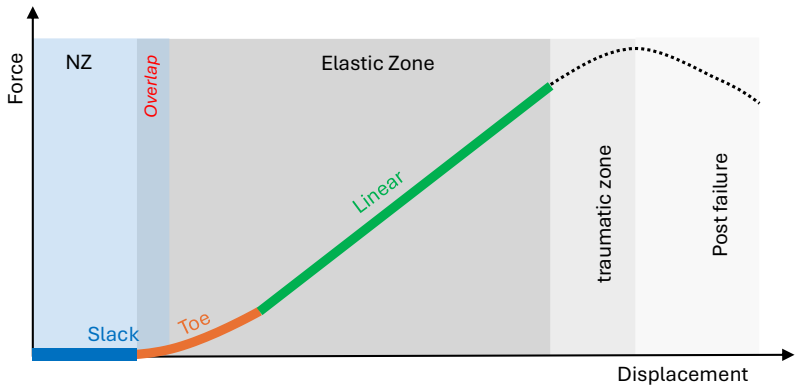


Figure 7 Schematic force–displacement response of a spinal ligament, showing the slack, toe and linear regions, followed by the traumatic zone and post-failure. The neutral zone (NZ) covers the slack region and overlaps the onset of the toe region.

Among the passive structures, the ligaments are considered to contribute most to the NZ (Panjabi, 1992). Loaded in tension, Figure 7, a ligament first elongates with little resistance (slack region), then stiffens as its crimped collagen fibres straighten (toe region), and responds near-linearly through the elastic zone before entering the traumatic zone and failing (Yoganandan *et al.*, 2000, Myklebust *et al.*, 1988, Chazal *et al.*, 1985, Mattucci *et al.*, 2012).

Injury Mechanisms and Classification

In a crash, the neck is loaded either inertially, when the head moves relative to the restrained torso, or by a head impact, when head motion is stopped while the torso continues (Svensson *et al.*, 2000, Foroutan *et al.*, 2024). Most neck injuries are AIS1 soft-tissue injuries, and the origin on tissue level still remains unclear (Siegmund *et al.*, 2009). In contrast, AIS2+ injuries are classified by the dominant loading mode at the time of failure (Allen *et al.*, 1982, Argenson *et al.*, 1997). Figure 8 summarizes the loading modes, the tissues involved and the resulting injuries.

In the lower cervical spine, compression loading mainly produces burst fractures of the vertebral body. Under compression–flexion loading, the anterior vertebral body fails first, giving wedge and teardrop fractures. Compression–extension loading mainly fractures the posterior elements, while lateral bending loading causes asymmetric compression of the vertebral body (Allen *et al.*, 1982). Under tension–flexion loading the posterior ligaments, the PLL and the disc fail from posterior to anterior, and rupture of the PLL marks the transition from a stable spine to an unstable injury (Argenson *et al.*, 1997). With increasing tension–flexion loading, the injury progresses from facet subluxation, through unilateral facet dislocation, to bilateral facet dislocation with anterior displacement of about half the vertebral body width (Allen *et al.*, 1982). Under tension–extension loading, the ALL and the anterior disc fail first. Combined axial rotation and lateral bending loading causes unilateral facet fractures and dislocations (Argenson *et al.*, 1997). Ligament failure is not visible on radiographs, so its extent is mainly inferred from vertebral displacement, which ranges from subluxation to complete dislocation. Isolated ligament injuries without fracture or dislocation are coded as AIS1 (Gennarelli and Wodzin, 2008).

The upper cervical spine injuries follow a separate injury pattern (Figure 8). Compression fractures the atlas (Jefferson fracture), and extension fractures the pedicles of C2 (Hangman's fracture). Tension causes atlantooccipital dislocation, axial rotation causes atlantoaxial rotatory dislocation, and shear causes dens fractures and transverse ligament rupture.

The classifications above suggest that ligaments may play a central role in the onset of these injuries. In both tension mechanisms, the earliest stage described is ligament failure without bony injury (Allen *et al.*, 1982), and facet dislocation appears to require prior disruption of the CL and PLL (Argenson *et al.*, 1997). In compression–flexion, bone fails first, but posterior ligament failure is also reported in the most severe

stages (Allen *et al.*, 1982). Ligament failure may therefore be an early event in several mechanisms and could contribute to the injury progression; from a stable to an unstable injury (Argenson *et al.*, 1997).

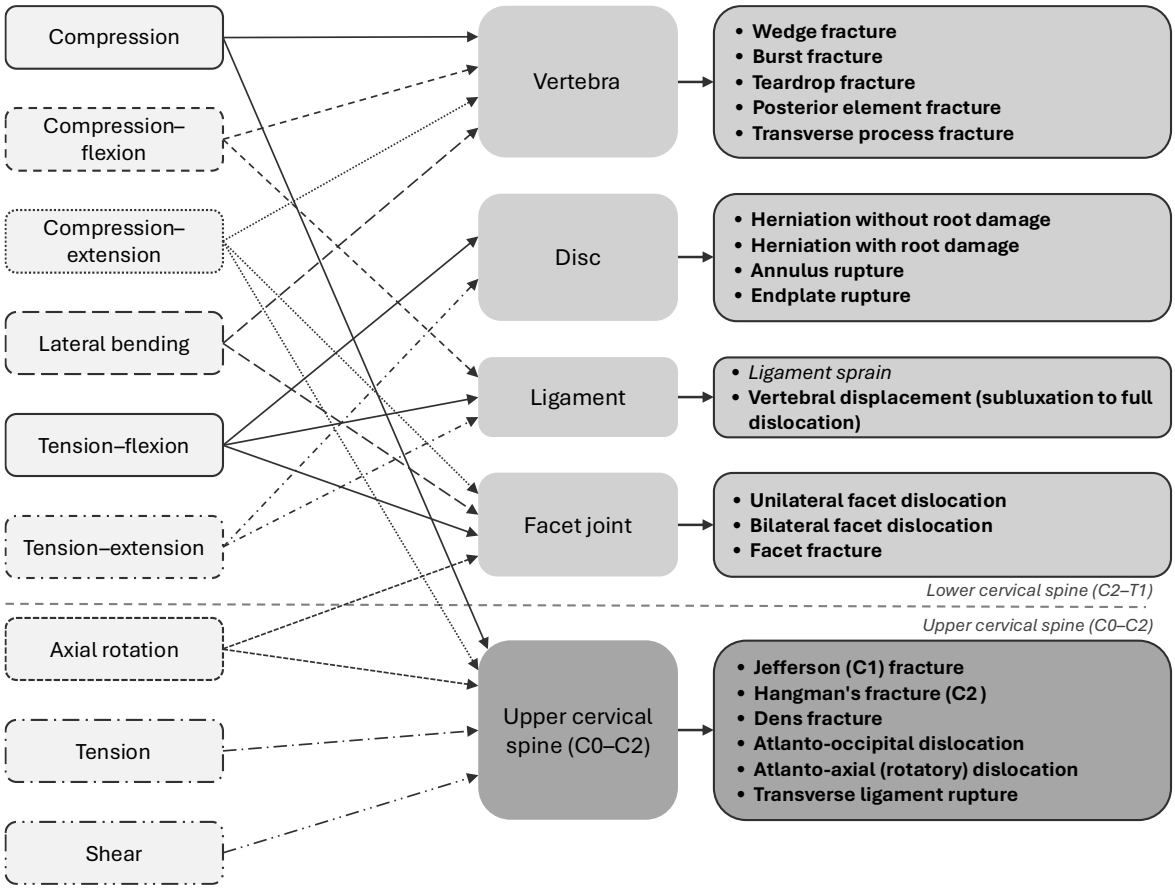


Figure 8 Injury mechanisms of the cervical spine: loading modes (left), injured tissues or regions (middle) and resulting injuries (right), separated into the lower (C2–T1) and upper (C0–C2) cervical spine. Injuries in bold are AIS2+ and injuries in italics AIS1 (Gennarelli and Wodzin, 2008). Based on (Allen *et al.*, 1982, Argenson *et al.*, 1997)

Finite Element Neck Models

Cervical spine models for impact biomechanics date back to multibody models of the head and neck (Deng and Goldsmith, 1987). Detailed multibody models, with rigid vertebrae connected by deformable discs, ligaments and muscles modelled as discrete elements, followed in the 1990s (de Jager, 1996). The first FE neck models were presented in the 1990s (Kleinberger, 1993, Yang *et al.*, 1998). These were followed by the model of the Royal Institute of Technology (KTH) model (Halldin *et al.*, 2000), the THUMS neck (Kitagawa *et al.*, 2006), and the University of Waterloo model, which forms the neck of the detailed GHBMC model (Panzer *et al.*, 2011). More recent models include the VIVA model (later also adopted in the VIVA+ model) (Östh *et al.*, 2016) and the University of Strasbourg (UNISTRA) model (Meyer *et al.*, 2021). A large number of head-neck FE models have since been developed and validated for both collision and medical applications (Liang *et al.*, 2025).

Cervical spine FE models have been applied in a wide range of fields, from medical research to injury biomechanics (Liang *et al.*, 2025). Medical models are used to study physiological loading, degeneration and surgical treatment, and therefore focus on anatomical detail under small deformations and quasi-static loading. Models for crash safety, such as those in the HBMs used for injury assessment, must capture large deformations under dynamic loading up to injury, and therefore require nonlinear, rate-dependent tissue properties.

The geometry of FE neck models is traditionally based on a single individual. The, GHBMC neck model is based on imaging of one 50th percentile male (Gayzik *et al.*, 2011) and the VIVA model on a single female

spine scaled to represent an average male (Östh *et al.*, 2016). Single individuals may differ considerably from the population it is intended to represent, so a geometry based on aggregated population data provides a more representative template. However, any single geometry, whether individual or average, cannot capture the effect of variability in vertebral geometry on the cervical spine response; this requires the template to be varied across the population.

The material properties of cervical spine FE models are derived from physical tests of isolated tissues. These tissues are nonlinear and viscoelastic, and their measured response varies between specimens and test methods, so different studies often report different properties for the same tissue (Cronin *et al.*, 2018). Cortical and trabecular bone are typically modelled as isotropic elastic–plastic materials, and the disc as a nucleus surrounded by an annulus of ground substance with embedded fibre layers (Cronin *et al.*, 2018, Östh *et al.*, 2016). The ligaments are modelled with tension-only truss elements (Panzer *et al.*, 2011) or nonlinear membrane elements (Östh *et al.*, 2016), using force–displacement curves from isolated ligament tests (Yoganandan *et al.*, 2000, Mattucci *et al.*, 2012, Mattucci *et al.*, 2013). Although the test data show large variability between specimens, the models use a single set of average properties (Cronin *et al.*, 2018, Östh *et al.*, 2016).

Most cervical spine FE models have been validated for quasi-static segmental RoM (Liang *et al.*, 2025) and some dynamic loading. The Waterloo model has been validated in frontal, rear and lateral impacts (Panzer *et al.*, 2011, Fice *et al.*, 2011, Barker *et al.*, 2017, Barker and Cronin, 2021, DeWit and Cronin, 2012) and against Function Spinal Unit (FSU) failure tests. The VIVA model has been validated in rear impacts (Östh *et al.*, 2016, Östh *et al.*, 2017), and the UNISTRA model against volunteer tests in frontal and lateral loading and PMHS tests in lateral impacts (Meyer *et al.*, 2021).

Injury Criteria

Cervical spine injury criteria can be divided into global criteria, based on forces, moments or accelerations, and local criteria, based on the response of individual structures. Local criteria can be defined at the organ level, for example from ligament force or elongation, or at the tissue level, from stress or strain within the tissue. They can further be deterministic, where injury is predicted when a given threshold is exceeded, or probabilistic, where the response is related to a risk of injury.

Cervical spine injury risk in crash testing is currently assessed with global criteria. The N_{ij} criterion was developed for AIS2+ injuries in frontal impacts. It combines the axial force and flexion-extension moment at the occipital condyles, each normalized by an intercept value specific to the ATD (Kleinberger *et al.*, 1998). The Neck Injury Criterion (NIC) was developed for AIS1 injuries in rear impacts. It combines the horizontal acceleration and velocity of the head relative to T1 (Boström *et al.*, 1997). The N_{km} criterion was also developed AIS 1 injuries rear impacts and combines the shear force and flexion-extension moment at the upper neck (Schmitt *et al.*, 2002).

Tolerance values and IRFs for the neck have been derived directly from tests on PMHS head–neck specimens in axial compression and tension (Nightingale *et al.*, 1996, Van Ee *et al.*, 2000), and more recently for lateral bending combined with axial head rotation (Yoganandan *et al.*, 2023). Meyer *et al.* (2021) derived model-specific IRFs from global neck loads with the UNISTRA model, relating upper and lower neck forces computed in simulations of PMHS lateral impact tests to injury. Being based on global loads, these criteria are specific to the loading direction for which they were developed, and do not directly indicate which structure is injured.

The current local criteria in HBMs are deterministic and differ between models in the structure assessed and the metric used. Using the Waterloo model, (Fice *et al.*, 2011, DeWit and Cronin, 2012, Shateri and Cronin, 2015) predicted vertebral fracture by element erosion at a failure strain, ligament failure by progressive strain-based failure, disc avulsion by a tiebreak contact, and capsular ligament strain. Using the KTH model, Halldin *et al.* (2000) predicted C2 fracture from bone stress, and (Brolin and Halldin, 2004, Hedenstierna, 2008) predicted ligament failure from elongation, which is less sensitive to loading rate than force. Other studies have used ligament force (van Lopik and Acar, 2004), von Mises stress in C1 (Teo and

Ng, 2001) and damage laws for bone (Mustafy *et al.*, 2014, Mustafy *et al.*, 2016). Criteria have also been proposed for the spinal cord (Liang, 2022) and the carotid arteries (Danelson *et al.*, 2009).

The thresholds in these criteria typically mean failure values from physical tests (Myklebust *et al.*, 1988, Yoganandan *et al.*, 2000, Mattucci *et al.*, 2012). However, a single threshold does not account for the variability in tissue tolerance across the population, and it only indicates whether the threshold is exceeded, not the risk of injury. Östh *et al.* (2017) partly addressed this in an analysis with the VIVA model, reporting the proportion of capsular ligament elements exceeding sub-catastrophic and catastrophic strain levels.

Survival Modelling for Injury Risk Functions

Survival modelling describes the time until an event occurs, such as injury, and is widely used in injury biomechanics. The survival function S(x) gives the probability that the event has not occurred by x (the time), and its complement to the cumulative distribution function F(x), gives the probability the event occurred, Equation (1):

$$F(x) = 1 - S(x) \tag{1}$$

This framework can be used to construct an Injury Risk Function (IRF) by replacing time with a mechanical response that increases monotonically during loading, such as force, elongation or strain (Kent and Funk, 2004). F(x) is then the probability of injury when the chosen response reaches value x. For a ligament IRF, at an organ level, injury prediction in the response is elongation or force. Since the response at failure is known exactly in these controlled tests the observation is treated as uncensored/exact. Otherwise, the observation is right-censored if the test is stopped before the ligament fails (RoM tests), left-censored if failure has already occurred (drop tests), and interval-censored if it is only known to lie between two measured responses.

Post-Mortem Human Subject (PMHS) data are typically limited in the number of specimens and often censored, and for such data parametric survival analysis is recommended (Petitjean *et al.*, 2012). A parametric distribution gives a continuous IRF and allows explanatory variables (covariates) to be included. Since the response at failure is strictly positive and the risk of failure at zero response should be zero, only distributions defined on positive values are considered, such as the Weibull (Equation 2), log-normal (Equation 3) and log-logistic (Equation 4) distributions. Earlier IRFs did not always meet this requirement, and some predict a non-zero risk at zero response.

$$F(x) = 1 - \exp\left(-\exp\left(\frac{\ln x - \mu}{\sigma}\right)\right) \tag{2}$$

$$F(x) = \Phi\left(\frac{\ln x - \mu}{\sigma}\right) \tag{3}$$

$$F(x) = \frac{1}{1 + \exp\left(-\frac{\ln x - \mu}{\sigma}\right)} \tag{4}$$

where μ and σ are the location and scale parameters of ln x, which set the position and the spread of the IRF on the response axis, and Φ is the standard normal cumulative distribution function. In all three distributions, ln x follows a standard distribution shifted by μ and stretched by σ. The distributions differ only in which standard distribution this is, a smallest extreme value distribution for the Weibull, a normal distribution for the log-normal and a logistic distribution for the log-logistic (Meeker *et al.*, 1998). The Weibull distribution in Equation 2 corresponds to the usual Weibull form with scale e^{μ} and shape $1/\sigma$. All three have two parameters but differ in shape when plotted against ln x: the log-normal and log-logistic distributions are symmetric, the latter with heavier tails, whereas the Weibull distribution is skewed towards low responses.

Covariates in the survival model can be included through a proportional hazard or an accelerated failure time (AFT) formulation. In a proportional hazards model, the covariates scale the hazard, i.e. the instantaneous risk of failure. In an AFT model, they instead multiply the response at failure, stretching or

compressing it by a constant factor. The Weibull distribution satisfies both formulations, whereas the log-normal and log-logistic distributions are only AFT models. The AFT formulation is used in this thesis, with each covariate adding a linear term to μ, which for a single covariate z_1 gives:

$$\mu = \beta_0 + \beta_{z1} z_1 \tag{5}$$

where β_0 is the intercept and $\beta_{z1}$the regression coefficient of z_1. A unit increase in z_1 thus multiplies the response at failure by $e^{\beta_{z1}}$, shifting the IRF along the response axis without changing its shape. Further covariates are added as additional terms in the same way.

Bayesian Fit of Survival Models

The survival models above assume that all observations are independent. When several tissue samples come from the same donor, their responses at failure are correlated, and this assumption no longer holds. A hierarchical model fitted in a Bayesian framework can account for this dependence. Let $x = (x_1, \dots, x_n)$ denote the observed responses at failure. In Bayesian fitting, the parameters of the survival model, collected in θ (for example β_0, $\beta_{z1}$and σ for log-normal), are treated as probability distributions rather than fixed values. Prior knowledge about the parameters, $p(\theta)$, is combined with the likelihood of the observed responses at failure, $p(\theta|x)$, given by the chosen distribution, to give the posterior distribution (Equation 6).

$$p(\theta|x) \propto p(x|\theta)p(\theta) \tag{6}$$

The posterior is typically sampled using Markov Chain Monte Carlo (MCMC) methods (Gelman *et al.*, 2013). Each posterior sample defines one IRF, and together the samples give the IRF with its credible interval directly, without relying on large-sample approximations, which suits the small samples typical of PMHS data (Cutcliffe *et al.*, 2012). In addition, in a PMHS data set several specimens are often tested from the same donor, resulting in them sharing the PMHS (source) characteristics such as tissue quality. This implies the responses at failure are clustered. Treating them as independent would overstate the information in the data and underpredict the uncertainty in the results. A hierarchical model accounts for this by adding a parameter that varies between PMHS (McElreath, 2018). For the log-normal model (Equation 3) with a varying intercept, μ of donor j becomes.

$$\mu_j = \beta_0 + \beta_{z_1} z_1 + u_j, \qquad u_j \sim N(0, \sigma_{PMHS}) \tag{7}$$

Where u_j is the effect of donor j on the logarithmic scale and σ_{PMHS} is the variability between PMHS. Each PMHSs effect is estimated partly from its own specimens and partly from all other PMHS, so a PMHS with few samples is pulled towards the average. The same fitted model results in three IRFs. For a PMHS *j* in the dataset it becomes,

$$F_j(x) = \Phi\left(\frac{\ln x - (\mu + u_j)}{\sigma}\right) \tag{8}$$

For an average donor, the effect is set to zero, and the IRF becomes,

$$F_{avgerage}(x) = \Phi\left(\frac{\ln x - \mu}{\sigma}\right) \tag{9}$$

For the population (out of the dataset used), whose effect is unknown, the IRF becomes,

$$F_{population}(x) = \Phi\left(\frac{\ln x - \mu}{\sigma_{population}}\right), \qquad \text{where } \sigma_{population} = \sqrt{\sigma^2 + {\sigma_{pmhs}}^2} \tag{10}$$

This population IRF is wider than the IRF for an average donor, and it is the relevant one when predicting the risk for an occupant not represented in the dataset building the IRF, and as such the recommended one to use together with the HBM.

CHAPTER 4

SUMMARY OF PAPER A

The aims of Paper A were to develop and validate a cervical spine FE model representing an average male, and to quantify how population variability in vertebral geometry and ligament properties influences cervical spine responses. The study consisted of three parts: model development, model validation and a population variability study, Figure 9.

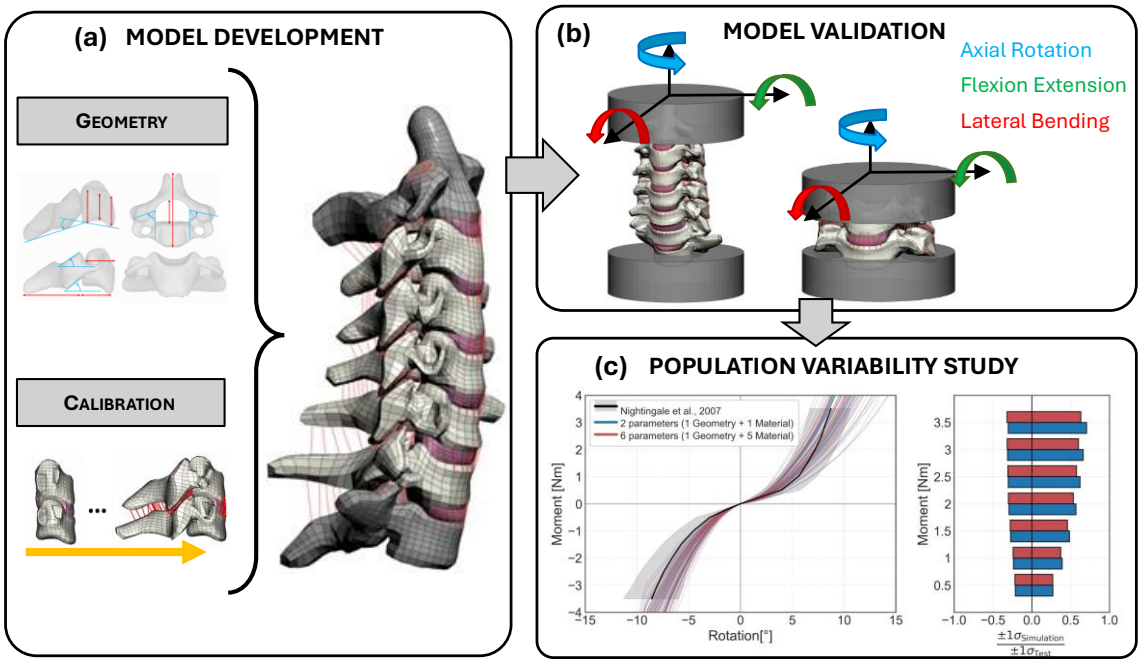


Figure 9 Overview of Study A. (a) Model development: morphing of the geometry to average male targets and calibration of the unstretched ligament lengths against stepwise-reduction tests. (b) Model validation in flexion-extension, lateral bending and axial rotation at LCS and FSU level. (c) Population variability study in flexion extension: C4–C5 moment-rotation responses of the sampled models compared with (Nightingale *et al.*, 2007) (left), and the ratio of simulated to experimental ±1 SD at each moment (right).

Methods

Model development (Figure 9a)

A cervical spine FE mesh, based on an 50th percentile male (Iraeus *et al.*, 2024), was morphed to fit aggregated average male dimensions from the literature. The morphing used global targets for the vertebral bodies and discs, and local targets for the facet joints. Variable cortical thickness was assigned based on the literature. The material properties of the annulus, nucleus and facet cartilage were calibrated using biomechanical data (Buchweitz *et al.*, 2025, Hori and Mockros, 1976). The ligament force–elongation properties were taken from tensile tests (Mattucci *et al.*, 2012) and the unstretched ligament lengths were calibrated. This calibration used stepwise-reduction tests, in which structures were removed one at a time (Jonas *et al.*, 2020). In the simulations, the structures were instead added one at a time, starting from the IVD alone, and ligament slack was introduced until the simulated RoM matched the experiments. The resulting model is referred to as the baseline model.

Model validation (Figure 9b)

The baseline model was validated against quasi-static pure moment tests in flexion-extension, lateral bending and axial rotation. Segmental RoM was compared at FSU level (Panjabi *et al.*, 2001, Wheeldon *et al.*, 2006, Nightingale *et al.*, 2007) and for the full LCS (Barrey *et al.*, 2015). Sagittal Instantaneous Centre of Rotations (ICRs) in flexion-extension were compared with experimental data (Jonas *et al.*, 2018).

Population variability study (Figure 9c)

The influence of variability was studied for the C4–C5 FSU in flexion-extension and compared with Nightingale *et al.* (2007). Vertebral geometry was varied using a single scaling parameter, and ligament material using scale factors on the ligament force. All were sampled from assumed normal distributions. Two hypotheses for the correlation between ligaments were tested: one geometry and one ligament parameter (fully correlated ligaments), or one geometry and five ligament parameters (fully independent ligament properties). Fifty samples were generated for the two groups and simulated in both flexion and extension, giving 2×2× (50+1) = 204 simulations including the baseline.

Results and Discussion

The morphed geometry matched the global targets and was within the reported ranges for the local targets and therefore represent a population average male. Calibration using the stepwise-reduction tests resulted in ligament slack of 0–2 mm, with the largest resulting values for the capsular ligaments. In lateral bending, the model was stiffer than the experiments already with the IVD alone. This may be related to the disc representation in the model. The detailed anatomy of the cervical annulus was not represented, and the tensile properties of the nucleus and annulus ground substance were not calibrated, as only compressive test data were available.

In the validation, the RoM of all FSUs from C2–C3 to C6–C7 was within the experimental corridors. In flexion–extension, the response was close to the experimental average, and the ICRs were within the experimental envelope. In axial rotation and lateral bending, the response deviated from the experiments at low moments, possibly because the model did not capture the full NZ reported in the experiments but fell within the corridors at higher moments. The RoM and ICR validation complemented each other, validating both the kinetics and kinematics of the model. For the whole lower cervical spine (C2–T1), the model was stiffer than the experiments in flexion and less stiff in extension above 1 Nm, possibly owing to differences in spinal curvature between the model and the specimens. The validation is, however, limited to quasi-static, non-injurious loading.

In the population study, the sampled models captured 27–71% of the experimental spread in flexion and 21–32% in extension (Figure 9c). Within the studied parameter ranges, vertebral geometry contributed more to the variability than ligament material properties. The lower values in extension may be explained by local geometry, such as facet orientation, which influences the extension response but was not varied in this study.

Overall, Paper showed that a lower cervical spine model with calibrated ligament slack can reproduce both the segmental kinetics and kinematics under quasi-static loading, and that population-level studies should at least include both vertebral geometric and ligament material variability.

CHAPTER 5

SUMMARY OF PAPER B

The aim of the study was to develop a ligament level IRF for cervical spine that accounts for the variation between individuals and can be used in HBMs. The study consisted of three parts: data analysis and variable selection and development of the IRF (Figure 10).

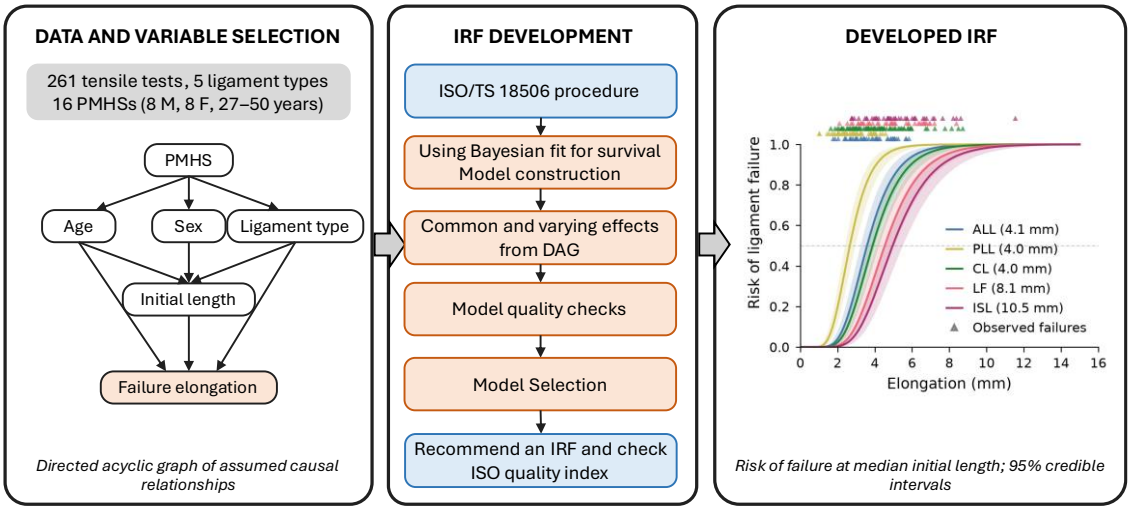


Figure 10 Overview of Paper B. (a) Data and assumed causal relationships between the variables, from which the model variables were selected. (b) Development of the IRF by extending the ISO/TS 18506 procedure (blue) with Bayesian survival modelling (orange). (c) Developed IRFs: risk of ligament failure against elongation for each ligament type at its median initial length, with 95% credible intervals.

Methods

Data and variable selection (Figure 10a)

The IRF was developed from 261 cervical ligament tensile tests on the ALL, PLL, CL, LF and ISL from 16 PMHSs (8 male, 8 female, 27–50 years) (Mattucci *et al.*, 2012). Since each PMHS contributed with several tests, the data were clustered i.e., all tests from one PMHS share the age and sex of that subject and cannot be treated as independent observations. To decide which variables to include, the assumed causal relationships between them were represented in a Directed Acyclic Graph (DAG) (Chen *et al.*, 2024). Based on the DAG, initial length, ligament type, age and sex were selected as candidate common effects on failure elongation, and PMHS as a varying effect.

IRF development (Figure 10b)

The ISO/TS 18506 procedure (Petitjean *et al.*, 2012) was adapted for hierarchical Bayesian models. Log-normal and Weibull models were built from the bottom up, from the candidate common and varying effects, giving 48 possible models. The models were compared using leave-one-out cross-validation (ELPD-LOO). The quality of the developed IRF was assessed with the ISO quality index.

Results and Discussion

The selected IRF, chosen from the 48 candidate models by their expected log density under leave-one-out cross validation (ELPD-LOO) is a log-normal model with ligament type, initial length and their interaction as common effects, also including a varying intercept for PMHS, and a varying effect for the left and right capsular ligaments of the same segment (Figure 10c). Its credible intervals were rated good by the ISO quality index for all ligament types, risk levels and initial lengths. Failure elongation increased with initial length, by about 14% per mm for the PLL, 12% for the LF, 6 % for the CL, 5% for the ISL and 2% for the ALL, with CrI including zero for CL and ALL. The elongation at 50% risk ranged from 2.7 mm for the PLL to 5.0 mm for the ISL.

The variation between PMHSs were small compared with the variation between tests (σ_{PMHS}= 0.090, σ = 0.305), and including age, sex or strain rate did not improve the predictions. The dependence between the left and right capsular ligaments of the same segment was accounted for by a varying effect for each pair ($\sigma_{CL} = 0.132$). This effect was small and did not change predictive accuracy (ΔELPD −0.55, SE 1.89) but was retained because the two ligaments of a pair are not independent. Most of the variation in failure elongation therefore appears to stem from the ligaments themselves rather than from the PMHS. One reason might be the narrow age range of the PMHS (27–50 years), which may have limited the differences in tissue properties between individuals. The variation between PMHS was nevertheless included in the IRF, since the 16 PMHS are a sample of the population, and an IRF intended for a new individual must account for the variation between PMHSs. The ISO step of checking the predictions against existing results was not performed, as it requires the IRF to be applied with a whole-body HBM, and will follow once the cervical spine model has been incorporated into one.

Overall, Paper B developed IRFs for the cervical spine ligaments from clustered data, using a hierarchical Bayesian workflow. The common and varying effects were selected from a causal structure. The recommended IRFs describe the risk of ligament failure for a new individual as a function of elongation, ligament type and initial length, and their credible intervals were rated good by the ISO quality index.

CHAPTER 6

DISCUSSION

In this licentiate thesis, steps were taken towards the main aim of advancing the prediction of moderate to more severe cervical spine injuries with HBMs in simulated MVCs. In Paper A, an average male lower cervical spine model was developed, with ligament slack calibrated against stepwise-reduction tests and the response was validated against RoM and ICR tests. Varying the model properties within the ranges of human variability showed that the vertebral geometry contributes more than ligament material to the variability in segmental response. In Paper B, the standard procedure for constructing IRFs was extended with a hierarchical Bayesian survival model, and a structured method to use clustered PMHS test data to construct IRF. The resulting IRF predicts the risk of ligament failure from elongation, for a given ligament type and initial length.

Ligament Initial Length

Local injury prediction in HBMs requires the elongation in the model to be measured from the same reference length as in the tests used to develop the IRF. Both papers in this thesis depend on this reference. In Paper A the initial lengths of the cervical spine ligaments were calibrated against stepwise reduction tests, which added a slack length that shifts the displacement at which each ligament begins to carry load. In Paper B, the risk of failure at a given elongation depended on the initial length measured before testing. To apply the IRF in an HBM, the slack must therefore be accounted for in the elongation, and the initial length must be defined as in the tests.

Compensation of the initial ligament length, applied as slack, is not specific to the model in Paper A but has been needed in other spine FE models. Initial ligament lengths were calibrated to match segmental responses in both lumbar (Iraeus *et al.*, 2023) and cervical spine models (Hadagali and Cronin, 2022). Ligament properties in these models are commonly derived from isolated tension tests, such as those of Chazal *et al.* (1985) and Mattucci *et al.* (2012). The slack thus reflects the difference between the tested (in vitro) and the in situ length of the ligament. Once isolated, a ligament is released from its anatomical constraints, and its unloaded length in the test does not necessarily correspond to its length in situ. The in situ length also varies between individuals and with posture. Any slack calibrated against FSU tests is therefore defined relative to the neutral position of the specimens, and it enters the risk predicted by a local IRF through the elongation, together with the uncertainty of the calibration.

But what is neutral position?

In biomechanical tests (FSU, ligamentous spine or full body), the kinematics of the tested unit is measured from the neutral position of that specimen. Tests report the neutral position as the position in which the specimen comes to rest after preparation and preconditioning (for an FSU) (Crawford *et al.*, 1998, Wilke *et al.*, 1998). That position, however, is a product of the test and it depends on how the specimen was prepared and preconditioned, and on any loads or constraints introduced by potting and mounting, and it varies between laboratories. In the living human, the neutral posture is not unique either: it differs between individuals and between repeated measurements in the same individual posture (Newell *et al.*, 2018), and it changes with posture. A model calibrated against FSU tests is, in effect, calibrated to a given posture and setup.

This uncertainty affects any calibration against FSU tests in which the reference position is not reported. In Paper A, it appeared in the stepwise-reduction calibration. Each step was assumed to start from the same position, yet removing a ligament can itself alter the neutral position of the FSU, so the reference from

which the slack was calibrated may have shifted between steps. This could not be accounted for in the simulations, as the starting position of each step was neither measured nor reported in the physical tests. Reporting the starting position of each step, together with spinal curvature and specimen geometry, would allow modelers to calibrate slack from a known reference, and would benefit any model calibrated against such tests.

HBMs are intended for a range of occupant postures, whereas ligament slack, as in Paper A, is calibrated for one, here a seated spinal curvature. In other postures, such as reclined seating or standing, the in-situ length of each ligament is unknown. One way to address this would be to describe the spinal curvature in each posture, from which the change in ligament length relative to the calibrated posture could be estimated in the model. This could be supplemented by ligament tests that record the in-situ length before the ligament is isolated, providing the reference length directly. Such data are, however, difficult to obtain, as they require either imaging of the spine in different postures or measurements on the specimen before dissection. Until they are available, how changes in ligament length with posture should enter ligament IRFs remains an open question.

Injury Risk Function

Cervical spine injury risk in HBMs is assessed in two ways. Global criteria describe the loading of the neck as a whole and were developed for ATDs or for specific HBMs, so they are not directly transferable to other HBMs. Local criteria use deterministic thresholds, which are implemented differently in each HBM. The IRFs developed in Paper B are instead derived directly from ligament tests and are therefore not tied to a particular model. They are also probabilistic, relating ligament elongation to a risk of failure. This model independence, however, holds only if the elongation in the model is defined as in the tests, which links it to the reference length uncertainties discussed in the previous section.

The recommended IRF in Paper B predicts ligament failure, whereas the most common AIS2+ cervical spine injuries are fractures and dislocations. Clinical studies indicate that dislocation is a progressive injury, starting with the failure of a single ligament and advancing as further ligaments of the segment fail (Allen *et al.*, 1982, Carrino *et al.*, 2006). Predicting this onset makes it possible to assess the risk of dislocation before it develops, in the same way as other injuries are predicted in HBMs from the failure of individual structures. Describing the progression towards a full dislocation would require a criterion that combines the risks of all ligaments in a segment, defined and validated against injury data.

Applying the IRF in an HBM also assumes that the model predicts ligament elongation correctly under the loading in which injuries occur. The model in Paper A was validated under quasi-static, non-injurious loading only. Its ligaments include rate-dependent properties, but their effect on the segmental response at crash-relevant loading rates has not been evaluated. The IRF in Paper B uses elongation as the response, assuming that strain rate affects failure force but not failure elongation. This assumption was supported within the tested range, as adding strain rate did not improve the predictions ($\Delta ELPD$ −1.15, SE 0.96). The role of loading rate therefore remains open mainly for the model in Paper A. Extending the model to injury prediction requires validation under dynamic loading and up to injurious levels, at both the segment and whole-spine level, and after integration into a whole-body HBM.

Further Applications

The methods developed in this thesis are transferable beyond the cervical spine model and the ligament IRF. The workflow in Paper B could be applied to IRFs for other tissues, and two of its elements make it particularly transferable. First, the common and varying effects are selected from a causal structure, which grounds the model in biomechanics rather than in statistical fit alone. Second, the hierarchical structure separates the variation between individuals from that within them, which allows the IRF to describe individuals beyond the tested specimens. The approach in Paper A, sampling variability in geometry and material around an average model, similarly shows how much of the experimental variability a model can represent before it is used across a population.

Ligament level prediction would allow cervical spine injury risk to be evaluated where global criteria do not apply, such as in postures and loading directions for which they were not developed. Combined with HBMs morphed to represent different subpopulations, it would allow restraint systems to be assessed for the occupants they protect, rather than for a single reference occupant.

The cervical spine model and the ligament IRF are also not tied to a specific loading environment, since the model represents the anatomy and tissue properties of the cervical spine and the IRF is based on tensile tests of isolated ligaments. They could therefore be used in other applications where neck injury is a concern, such as falls, sports impacts and helmet design. Extending them to these applications would require validation under the relevant loading conditions, particularly where these differ substantially from those in MVCs.

Beyond the Average Male

The modelling approach in Paper A is not limited to the average male it was developed for, and can be used to represent other populations, such as females or occupants of different sizes and ages. The average male was used because most anatomical and experimental data on the cervical spine come from male subjects. In Paper A, the vertebral geometry was morphed to literature-based targets. Further, morphing was used to generate a population of models, which captured part of the experimental scatter in segmental response. The average male model can thus serve as a template for other targets, for example those of a female cervical spine. The response of such a model can then be compared with and validated against test data for the corresponding population. The IRFs in Paper B can be applied to such models directly, as they are local criteria based on ligament elongation and contain no terms specific to sex or age. Differences between populations then enter through the geometry, that is, through the initial length and the elongation predicted by the model. The model developed in this thesis therefore provides a starting point for predicting cervical spine injuries in other populations.

CHAPTER 7

CONCLUSIONS

This licentiate thesis addressed the first two objectives of the PhD project, to develop, calibrate and validate a ligamentous model of the lower cervical spine and evaluate how population variability affects its response, and to develop a ligament injury risk function for the cervical spine for injury prediction with human body models.

For the first objective, a finite element model of an average male lower cervical spine was developed, with vertebral geometry morphed to literature-based targets at both global and local levels. Ligament slack was calibrated against stepwise reduction tests, and the model responses fell within the experimental corridors of independent validation data for range of motion and instantaneous centres of rotation. Introducing population variability captured 22–71% of the experimental spread in range of motion flexion-extension, with vertebral geometry contributing more than ligament material properties. The model thus represents the quasi-static response of the average male lower cervical spine, and geometric and ligament variability should be accounted for in population-based simulations. The calibrated slack, however, is defined relative to the neutral position of the tested specimens, so applying the model to other postures requires the slack to be re-established for each posture.

For the second objective, a population-level injury risk function for the cervical spine ligaments was developed, using a workflow that extends the standard procedure with a hierarchical Bayesian survival model and selection of variables from a causal structure. The function predicts the risk of ligament failure from elongation for a given ligament type and initial length, which together explained most of the variation in failure elongation, whereas the variation between PMHS was small. Since the hierarchical model separates the variation between individuals from that within them, the function can describe the risk for occupants beyond the tested specimens. Its use in an HBM, however, depends on how the initial length and elongation are defined, and therefore requires them to be defined consistently between model and tests, including the slack.

By combining a calibrated ligamentous lower cervical spine model that captures population variability with ligament IRFs, this thesis takes a step in advancing the prediction of moderate to severe neck injuries in motor vehicle crashes, enabling the development of even more efficient countermeasures.

CHAPTER 8

FUTURE WORK

Beyond this licentiate thesis, the model will be extended to the upper cervical spine, and the full cervical spine will be validated under dynamic and injurious loading (Objective 3). These validations are needed before the model can be used for injury prediction in MVCs, since the present validation is limited to quasistatic and non-injurious loading.

The next step is to move from the failure of individual ligaments to the injury of a segment (Objective 4). The present IRF predicts the failure of a single ligament, and how the failures of several ligaments combine into a segment injury is yet to be established. Allen *et al.* (1982) described dislocations as a staged progression. In hyperflexion, for example, the posterior ligaments fail first and the facets partially dislocate, followed by unilateral and then bilateral facet dislocation. Since each stage involves the failure of more ligaments, injury severity increases with the number of failed ligaments, which offers a way to combine the ligament risks into a segment-level prediction of clinical injury.

A criterion for vertebral fracture could complement the ligament IRFs in predicting AIS2+ cervical spine injuries. As shown by the epidemiology, compression fractures of the vertebral body are among the most frequent of these injuries. To the author's knowledge, the involvement of the ligaments in compression fractures is not well documented. Moreover, (Myers and Winkelstein, 1995) showed that the surrounding soft tissues create an additional load path that affects the kinematics of the spine and, through it, the injury risk. Their representations and passive behaviours will therefore be evaluated and updated.

The work will then extend to the whole body (Objective 5). The model and the IRF will be incorporated in a full-body human body model and validated against recent whole-body tests that span impact directions, severities and occupant sizes (Crandall, 2015, Espelien *et al.*, 2026, Finfrock *et al.*, 2026). In the full body, the surrounding soft tissues create an additional load path that affects the kinematics of the spine and, through it, the injury risk. Their representations and passive behaviours will therefore be evaluated and updated.

REFERENCES

Al-Salehi, L., Kroeker, S. G., Kerrigan, J. R., Cripton, P. A., Panzer, M. B. & Siegmund, G. P. 2024. Cervical vertebral and spinal cord injuries in rollover occupants. *Injury Epidemiology,* 11**,** 30.

Allen, B. L., Jr., Ferguson, R. L., Lehmann, T. R. & O'Brien, R. P. 1982. A mechanistic classification of closed, indirect fractures and dislocations of the lower cervical spine. *Spine (Phila Pa 1976),* 7**,** 1-27.

Argenson, C., de Peretti, F., Ghabris, A., Eude, P., Lovet, J. & Hovorka, I. 1997. Classification des traumatismes du rachis cervical inférieur. *European Journal of Orthopaedic Surgery & Traumatology,* 7**,** 215-229.

Barker, J. B. & Cronin, D. S. 2021. Multilevel validation of a male neck finite element model with active musculature. *Journal of Biomechanical Engineering,* 143**,** 011005.

Barker, J. B., Cronin, D. S. & Nightingale, R. W. 2017. Lower Cervical Spine Motion Segment Computational Model Validation: Kinematic and Kinetic Response for Quasi-Static and Dynamic Loading. *Journal of Biomechanical Engineering,* 139.

Barrey, C., Rousseau, M. A., Persohn, S., Campana, S., Perrin, G. & Skalli, W. 2015. Relevance of using a compressive preload in the cervical spine: an experimental and numerical simulating investigation. *Eur J Orthop Surg Traumatol,* 25 Suppl 1**,** S155-65.

Bogduk, N. & Mercer, S. 2000. Biomechanics of the cervical spine. I: Normal kinematics. *Clinical Biomechanics,* 15**,** 633-648.

Boström, O., Svensson, M. Y., Aldman, B., Hansson, H. A., Håland, Y., Lövsund, P., Seeman, T., Suneson, A., Säljö, A. & Örtengren, T. A new neck injury criterion candidate-based on injury findings in the cervical spinal ganglia after experimental neck extension trauma. Proceedings Of The 1996 International IRCOBI Conference on the Biomechanics of Impact, September 11-13, 1996, Dublin, Ireland, 1997.

Brolin, K. & Halldin, P. 2004. Development of a Finite Element Model of the Upper Cervical Spine and a Parameter Study of Ligament Characteristics. *Spine,* 29**,** 376-385.

Buchweitz, N., Sun, Y., Kelley, J., Porto, S. C., Wang, S., Reitman, C. A., Yao, H. & Wu, Y. 2025. Characterizing the Baseline Regional Biphasic Mechanical Properties of Cervical Intervertebral Discs. *Ann Biomed Eng*.

Buwaider, A., El-Hajj, V. G., Blixt, S., Nilsson, G., MacDowall, A., Gerdhem, P., Edstrom, E. & Elmi-Terander, A. 2024. Predictors of early mortality following surgical or nonsurgical treatment of subaxial cervical spine fractures: a retrospective nationwide registry study. *Spine J,* 24**,** 1939-1951.

Carlsson, A., Chang, F., Lemmen, P., Kullgren, A., Schmitt, K.-U., Linder, A. & Svensson, M. Y. EvaRID - A 50th Percentile Female Rear Impact Finite Element Dummy Model. Proceedings of the 2012 International Research Council on Biomechanics of Injury (IRCOBI) Conference, 2012/09/12 2012 Dublin, Ireland. 249-262.

Carrino, J. A., Manton, G. L., Morrison, W. B., Vaccaro, A. R., Schweitzer, M. E. & Flanders, A. E. 2006. Posterior longitudinal ligament status in cervical spine bilateral facet dislocations. *Skeletal radiology,* 35**,** 510-514.

Chazal, J., Tanguy, A., Bourges, M., Gaurel, G., Escande, G., Guillot, M. & Vanneuville, G. 1985. Biomechanical properties of spinal ligaments and a histological study of the supraspinal ligament in traction. *Journal of Biomechanics,* 18**,** 167-176.

Chen, G., Cai, Z. & Taylor, P. A. 2024. Through the lens of causal inference: Decisions and pitfalls of covariate selection. *Aperture Neuro,* 4**,** 10.52294/001c. 124817.

Claytor, B., MacLennan, P. A., McGwin, G., Jr., Rue, L. W., 3rd & Kirkpatrick, J. S. 2004. Cervical spine injury and restraint system use in motor vehicle collisions. *Spine (Phila Pa 1976),* 29**,** 386-9; discussion Z2.

Crandall, J. 2015. ATD Thoracic response test development Gold standard test 2: force limit belt 30Km/h Frontal. Cooperative Agreem nt No. DT NH22-09-H-0027.

Crawford, N. R., Peles, J. D. & Dickman, C. A. 1998. The spinal lax zone and neutral zone: measurement techniques and parameter comparisons. *J Spinal Disord,* 11**,** 416-29.

Cronin, D. S., Singh, D., Gierczycka, D., Barker, J. & Shen, D. 2018. Modeling the neck for impact scenarios. *Basic Finite Element Method as Applied to Injury Biomechanics.* Elsevier.

Cutcliffe, H. C., Schmidt, A. L., Lucas, J. E. & Bass, C. R. D. 2012. How Few? Bayesian Statistics in Injury Biomechanics. The Stapp Association.

Danelson, K. A., Gayzik, F. S., Yu, M. M., Martin, R. S., Duma, S. M. & Stitzel, J. D. 2009. Bilateral carotid artery injury response in side impact using a vessel model integrated with a human body model. *Annals of Advances in Automotive Medicine,* 53**,** 271-279.

Davidsson, J. 1999. BioRID II final report. Göteborg, Sweden: Crash Safety Division, Department of Machine and Vehicle Design, Chalmers University of Technology.

de Jager, M. K. J. 1996. *Mathematical head-neck models for acceleration impacts.* PhD thesis, Eindhoven University of Technology.

Deng, Y. C. & Goldsmith, W. 1987. Response of a human head/neck/upper-torso replica to dynamic loading—II. Analytical/numerical model. *Journal of Biomechanics,* 20**,** 487-497.

DeWit, J. A. & Cronin, D. S. 2012. Cervical spine segment finite element model for traumatic injury prediction. *Journal of the Mechanical Behavior of Biomedical Materials,* 10**,** 138-150.

Dutschke, J., Hutchinson, T., Jones, C. & Lindsay, V. L. 2023. *Car drivers with an AIS2+ spine injury: Description of a sample from South Australia*, Centre for Automotive Safety Research, The University of Adelaide.

Espelien, C., Donlon, J. P., Shin, J., Gallaher, M., Sochor, S., Noss, J., Carpenter, R., Cemborain, P. G. & Forman, J. 2026. Neck Motion and Injuries of Small Females and Midsize Males in Frontal Impacts at Two Severities. *Ann Biomed Eng*.

Fice, J. B., Cronin, D. S. & Panzer, M. B. 2011. Cervical spine model to predict capsular ligament response in rear impact. *Ann Biomed Eng,* 39**,** 2152-62.

Finfrock, R., Bendig, A., Thomas, C., Millis, W., Moorhouse, K. & Kang, Y.-S. Cervical Intervertebral Motion as a Soft-Tissue Injury Predictor for Neck Hyperextension in Low-SpeedRear Impacts. IRCOBI Conference, 2026 Munich, Germany. International Research Council on the Biomechanics of Injury.

Fontes, R. B. d. V., Baptista, J. S., Rabbani, S. R., Traynelis, V. C. & Liberti, E. A. 2015. Structural and ultrastructural analysis of the cervical discs of young and elderly humans. *PLoS One,* 10**,** e0139283.

Foroutan, P., Quarrington, R. D. & Jones, C. F. 2024. Mechanisms and risk factors associated with spinal cord injury, facet fracture, and level of dislocation, in occupants with cervical spine dislocations sustained in motor vehicle crashes. *Traffic Inj Prev,* 25**,** 1129-1136.

Freeman, M. D. & Leith, W. M. 2020. Estimating the number of traffic crash-related cervical spine injuries in the United States; An analysis and comparison of national crash and hospital data. *Accident Analysis & Prevention,* 142**,** 105571.

Gayzik, F. S., Moreno, D. P., Geer, C. P., Wuertzer, S. D., Martin, R. S. & Stitzel, J. D. 2011. Development of the Global Human Body Models Consortium Mid-Sized Male Full Body Model.

Gelman, A., Carlin, J. B., Stern, H. S., Dunson, D. B., Vehtari, A. & Rubin, D. B. 2013. *Bayesian Data Analysis,* Boca Raton, Florida, CRC Press.

Gennarelli, T. A. & Wodzin, E. 2008. Abbreviated injury scale 2005: update 2008. *Russ Reeder,* 200.

Gray, H. 1918. Antomy of the human body. *Annals of surgery,* 68**,** 564-566.

Hadagali, P. & Cronin, D. S. 2022. Enhancing the biofidelity of an upper cervical spine finite element model within the physiologic range of motion and its effect on the full ligamentous neck model response. *Journal of Biomechanical Engineering,* 145**,** 011010.

Halldin, P. H., Brolin, K., Kleiven, S., von Holst, H., Jakobsson, L. & Palmertz, C. 2000. Investigation of conditions that affect neck compression-flexion injuries using numerical techniques. *Stapp Car Crash J,* 44**,** 127-138.

Hedenstierna, S. 2008. *3D finite element modeling of cervical musculature and its effect on neck injury prevention*. KTH.

Hori, R. Y. & Mockros, L. 1976. Indentation tests of human articular cartilage. *Journal of Biomechanics,* 9**,** 259-268.

Huelke, D. F., Mackay, G. M., Morris, A. & Bradford, M. 1993. A review of cervical fractures and fracture-dislocations without head impacts sustained by restrained occupants. *Accident Analysis & Prevention,* 25**,** 731-743.

Inamasu, J. & Kato, M. 2018. Airbag deployment and cervical spine injury in restrained drivers following motor vehicle collisions. *Neuroradiology,* 60**,** 1307-1313.

Iraeus, J., Brynskog, E., John, J., Östh, J., Pipkorn, B. & Davidsson, J. 2024. Development of SAFER HBM v11. *Chalmers digital repository https://research.chalmers.se/publication/544460,* 2024:06, Version 1.1.

Iraeus, J., Poojary, Y. N., Jaber, L., John, J. & Davidsson, J. A new open-source finite element lumbar spine model, its tuning and validation, and development of a tissue-based injury risk function for compression fractures. IRCOBI Conference, 2023 Cambridge, United Kingdom.

Isopi, D. J., Depinet, P. J., Steinhour, A., Loeber, B. & Greenlees, B. EvaRID-50th Percentile Female Biofidelity Evaluation Assessed Against Volunteers in a Low-Speed Rear Impact. Proceedings of the 2026 International Research Council on Biomechanics of Injury (IRCOBI) Conference, 2026/09/09 2026 Munich, Germany.

John, J., Klug, C., Kranjec, M., Svenning, E. & Iraeus, J. 2022. Hello, world! VIVA+: A human body model lineup to evaluate sex-differences in crash protection. *Frontiers in bioengineering and biotechnology,* 10**,** 918904.

Jonas, R., Demmelmaier, R., Hacker, S. P. & Wilke, H. J. 2018. Comparison of three-dimensional helical axes of the cervical spine between in vitro and in vivo testing. *Spine J,* 18**,** 515-524.

Jonas, R., Demmelmaier, R. & Wilke, H. J. 2020. Influences of functional structures on the kinematic behavior of the cervical spine. *Spine J,* 20**,** 2014-2024.

Kapandji, A. I. 1974. *The physiology of the joints. Volume 3. The trunk and the vertebral column*.

Kent, R. W. & Funk, J. R. Data censoring and parametric distribution assignment in the development of injury risk functions from biochemical data. 2004 SAE World Congress, 2004.

Kitagawa, Y., Yasuki, T. & Hasegawa, J. 2006. A Study of Cervical Spine Kinematics and Joint Capsule Strain in Rear Impacts using a Human FE Model. The Stapp Association.

Kleinberger, M. 1993. Application of finite element techniques to the study of cervical spine mechanics.

Kleinberger, M., Sun, E., Eppinger, R., Kuppa, S. & Saul, R. 1998. Development of improved injury criteria for the assessment of advanced automotive restraint systems. *NHTSA Docket,* 4405**,** 12-17.

Larsson, K. J., Osth, J., Iraeus, J. & Pipkorn, B. 2024. A First Step Toward a Family of Morphed Human Body Models Enabling Prediction of Population Injury Outcomes. *J Biomech Eng,* 146.

Leledakis, A., Östh, J., Davidsson, J. & Jakobsson, L. 2021. The influence of car passengers' sitting postures in intersection crashes. *Accident Analysis & Prevention,* 157**,** 106170.

Liang 2022. Quantitative cervical spine injury responses in whiplash loading with a numerical method of natural neural reflex consideration. *Computer Methods and Programs in Biomedicine*.

Liang, Z., Wu, K., Tian, T. & Mo, F. 2025. Human head–neck model and its application thresholds: a narrative review. *International Journal of Surgery,* 111**,** 1042-1070.

Mattucci, S. F., Moulton, J. A., Chandrashekar, N. & Cronin, D. S. 2012. Strain rate dependent properties of younger human cervical spine ligaments. *Journal of the mechanical behavior of biomedical materials,* 10**,** 216-226.

Mattucci, S. F., Moulton, J. A., Chandrashekar, N. & Cronin, D. S. 2013. Strain rate dependent properties of human craniovertebral ligaments. *Journal of the mechanical behavior of biomedical materials,* 23**,** 71-79.

McElreath, R. 2018. *Statistical rethinking: A Bayesian course with examples in R and Stan*, chapman and hall/cRc.

McMurry, T. L., Poplin, G. S., Shaw, G. & Panzer, M. B. 2018. Crash safety concerns for out-of-position occupant postures: A look toward safety in highly automated vehicles. *Traffic Inj Prev,* 19**,** 582-587.

Meeker, W. Q., Escobar, L. A. & Pascual, F. G. 1998. *Statistical methods for reliability data*, Wiley, New York.

Mercer, S. & Bogduk, N. 1999. The Ligaments and Anulus Fibrosus of Human Adult Cervical Intervertebral Discs. *Spine,* 24**,** 619-626.

Mercer, S. R. & Bogduk, N. 2003. Clinical anatomy of ligamentum nuchae. *Clinical Anatomy,* 16**,** 484-493.

Meredith, L., Kovaceva, J. & Balint, A. 2020. Mapping fractures from traffic accidents in Sweden: How do cyclists compare to other road users? *Traffic Inj Prev,* 21**,** 209-214.

Meyer, F., Humm, J., Yoganandan, N., Leszczynski, A., Bourdet, N., Deck, C. & Willinger, R. 2021. Development of a detailed human neck finite element model and injury risk curves under lateral impact. *J Mech Behav Biomed Mater,* 116**,** 104318.

Müller, C. W., Otte, D., Decker, S., Stübig, T., Panzica, M., Krettek, C. & Brand, S. 2014. Vertebral fractures in motor vehicle accidents–a medical and technical analysis of 33,015 injured front-seat occupants. *Accident Analysis & Prevention,* 66**,** 15-19.

Mustafy, T., El-Rich, M., Mesfar, W. & Moglo, K. 2014. Investigation of impact loading rate effects on the ligamentous cervical spinal load-partitioning using finite element model of functional spinal unit C2-C3. *Journal of Biomechanics,* 47**,** 2891-2903.

Mustafy, T., Moglo, K., Adeeb, S. & El-Rich, M. 2016. Injury mechanisms of the ligamentous cervical C2-C3 functional spinal unit to complex loading modes: finite element study. *Journal of the Mechanical Behavior of Biomedical Materials,* 53**,** 384-396.

Myers, B. S. & Winkelstein, B. A. 1995. Epidemiology, classification, mechanism, and tolerance of human cervical spine injuries. *Critical Reviews™ in Biomedical Engineering,* 23.

Myklebust, J. B., Pintar, F., Yoganandan, N., CUSICK, J. F., Maiman, D., MYERS, T. J. & Sances Jr, A. 1988. Tensile strength of spinal ligaments. *Spine,* 13**,** 528-531.

Newell, R. S., Blouin, J.-S., Street, J., Cripton, P. A. & Siegmund, G. P. 2018. The neutral posture of the cervical spine is not unique in human subjects. *Journal of Biomechanics,* 80**,** 53-62.

Nightingale, R. W., Chancey, V. C., Ottaviano, D., Luck, J. F., Tran, L., Prange, M. & Myers, B. S. 2007. Flexion and extension structural properties and strengths for male cervical spine segments. *Journal of biomechanics,* 40**,** 535-542.

Nightingale, R. W., McElhaney, J. H., Richardson, W. J., Best, T. M. & Myers, B. S. 1996. Experimental impact injury to the cervical spine: relating motion of the head and the mechanism of injury. *JBJS,* 78**,** 412-21.

NSCISC. 2025. *National Spinal Cord Injury Statistical Center* Available: https://sites.uab.edu/nscisc/.

Östh, J., Bohman, K. & Jakobsson, L. Whole-Sequence Rear-End Impact Simulations with an Active Human Body Model. Conference proceedings International Research Council on the Biomechanics of Injury, IRCOBI, 2025.

Östh, J., Brolin, K., Svensson, M. Y. & Linder, A. 2016. A Female Ligamentous Cervical Spine Finite Element Model Validated for Physiological Loads. *Journal of Biomechanical Engineering,* 138.

Östh, J., Mendoza-Vazquez, M., Sato, F., Svensson, M. Y., Linder, A. & Brolin, K. 2017. A female head–neck model for rear impact simulations. *Journal of biomechanics,* 51**,** 49-56.

Oxland, T. R. & Panjabi, M. M. 1992. The onset and progression of spinal injury: A demonstration of neutral zone sensitivity. *Journal of Biomechanics,* 25**,** 1165-1172.

Pal, G. P., Routal, R. V. & Saggu, S. K. 2001. The orientation of the articular facets of the zygapophyseal joints at the cervical and upper thoracic region. *Journal of Anatomy,* 198**,** 431-441.

Panjabi, M., DVORAK, J., DURANCEAU, J., YAMAMOTO, I., GERBER, M., RAUSCHNING, W. & BUEFF, H. U. 1988. Three-Dimensional Movements of the Upper Cervical Spine. *Spine,* 13**,** 726-730.

Panjabi, M. M. 1992. The stabilizing system of the spine. Part II. Neutral zone and instability hypothesis. *Clinical Spine Surgery,* 5**,** 390-397.

Panjabi, M. M., Crisco, J. J., Vasavada, A., Oda, T., Cholewicki, J., Nibu, K. & Shin, E. 2001. Mechanical properties of the human cervical spine as shown by three-dimensional load–displacement curves. *Spine,* 26**,** 2692-2700.

Panjabi, M. M., Oxland, T., Takata, K., Goel, V., Duranceau, J. & Krag, M. 1993. Articular facets of the human spine quantitative three-dimensional anatomy. *Spine,* 18**,** 1298-1310.

Panjabi, M. M., White III, A. & Johnson, R. 1975. Cervical spine mechanics as a function of transection of components. *Journal of biomechanics,* 8**,** 327-336.

Panzer, M. B., Fice, J. B. & Cronin, D. S. 2011. Cervical spine response in frontal crash. *Medical Engineering & Physics,* 33**,** 1147-1159.

Petitjean, A., Trosseille, X., Praxl, N., Hynd, D. & Irwin, A. 2012. Injury risk curves for the WorldSID 50 th male dummy. SAE Technical Paper.

Pipkorn, B., Iraeus, J., Lindkvist, M., Puthan, P. & Bunketorp, O. 2020. Occupant injuries in light passenger vehicles—A NASS study to enable priorities for development of injury prediction capabilities of human body models. *Accident Analysis & Prevention,* 138**,** 105443.

Quarrington, R. D., Jones, C. F., Tcherveniakov, P., Clark, J. M., Sandler, S. J. I., Lee, Y. C., Torabiardakani, S., Costi, J. J. & Freeman, B. J. C. 2018. Traumatic subaxial cervical facet subluxation and dislocation: epidemiology, radiographic analyses, and risk factors for spinal cord injury. *Spine J,* 18**,** 387-398.

Rudd, R. W. & Parenteau, C. S. Serious spine injuries using 2017–2021 CISS and CIREN data: effect of spinal degeneration comorbidities. IRCOBI Conference, 2023.

Schaefer, L. C., Junge, M., Voros, I., Kocaslan, K. & Becker, U. 2021. Odds ratios for reclined seating positions in real-world crashes. *Accid Anal Prev,* 161**,** 106357.

Schmitt, K.-U., Muser, M. H., Walz, F. H. & Niederer, P. F. 2002. N km--a proposal for a neck protection criterion for low-speed rear-end impacts. *Traffic injury prevention,* 3**,** 117-126.

Shateri, H. & Cronin, D. S. 2015. Out-of-Position Rear Impact Tissue-Level Investigation Using Detailed Finite Element Neck Model. *Traffic Inj Prev,* 16**,** 698-708.

Shigeta, K., Kitagawa, Y. & Yasuki, T. Development of next generation human body FE model capable of organ injury prediction. Proceedings: International Technical Conference on the Enhanced Safety of Vehicles, 2009. National Highway Traffic Safety Administration.

Siegmund, G. P., Winkelstein, B. A., Ivancic, P. C., Svensson, M. Y. & Vasavada, A. 2009. The Anatomy and Biomechanics of Acute and Chronic Whiplash Injury. *Traffic Injury Prevention,* 10**,** 101-112.

Svensson, M. Y., Boström, O., Davidsson, J., Hansson, H.-A., Håland, Y., Lövsund, P., Suneson, A. & Säljö, A. 2000. Neck injuries in car collisions—a review covering a possible injury mechanism and the development of a new rear-impact dummy. *Accident Analysis & Prevention,* 32**,** 167-175.

Teo, E. & Ng, H. 2001. Evaluation of the role of ligaments, facets and disc nucleus in lower cervical spine under compression and sagittal moments using finite element method. *Medical engineering & physics,* 23**,** 155-164.

Tonetti, J., Potton, L., Riboud, R., Peoc'h, M., Passagia, J. G. & Chirossel, J. P. 2005. Morphological cervical disc analysis applied to traumatic and degenerative lesions. *Surgical and Radiologic Anatomy,* 27**,** 192-200.

Utheim, N. C., Helseth, E., Stroem, M., Rydning, P., Mejlænder-Evjensvold, M., Glott, T., Hoestmaelingen, C. T., Aarhus, M., Roenning, P. A. & Linnerud, H. 2022. Epidemiology of traumatic cervical spinal fractures in a general Norwegian population. *Injury Epidemiology,* 9**,** 10.

Van Ee, C. A., Nightingale, R. W., Camacho, D. L., Chancey, V. C., Knaub, K. E., Sun, E. A. & Myers, B. S. 2000. Tensile properties of the human muscular and ligamentous cervical spine. *Stapp Car Crash J,* 44**,** 85-102.

van Lopik, D. W. & Acar, M. 2004. A computational model of the human head and neck system for the analysis of whiplash motion. *International Journal of Crashworthiness,* 9**,** 465-473.

Waseem, M., Torlincasi, A. M. & Hall, W. A. 2025. Cervical Injury. *StatPearls*. Treasure Island (FL): StatPearls Publishing

Wheeldon, J. A., Pintar, F. A., Knowles, S. & Yoganandan, N. 2006. Experimental flexion/extension data corridors for validation of finite element models of the young, normal cervical spine. *Journal of biomechanics,* 39**,** 375-380.

Wilke, H.-J., Wenger, K. & Claes, L. 1998. Testing criteria for spinal implants: recommendations for the standardization of in vitro stability testing of spinal implants. *European spine journal,* 7**,** 148-154.

Womack, W., Woldtvedt, D. & Puttlitz, C. M. 2008. Lower cervical spine facet cartilage thickness mapping. *Osteoarthritis and Cartilage,* 16**,** 1018-1023.

Yang, K. H., Zhu, F., Luan, F., Zhao, L. & Begeman, P. C. Development of a finite element model of the human neck. Proceedings of the 42nd Stapp Car Crash Conference, 1998.

Yoganandan, N., Baisden, J., Vedantam, A. & Banerjee, A. 2023. Complex Neck Loading and Injury Tolerance in Lateral Bending With Head Rotation From Human Cadaver Tests1. *Journal of Engineering and Science in Medical Diagnostics and Therapy,* 7.

Yoganandan, N., Haffner, M., Maiman, D. J., Nichols, H., Pintar, F. A., Jentzen, J., Weinshel, S. S., Larson, S. J. & Sances, A. 1989. Epidemiology and Injury Biomechanics of Motor Vehicle Related Trauma to the Human Spine. SAE International.

Yoganandan, N., Kumaresan, S. & Pintar, F. A. 2000. Geometric and mechanical properties of human cervical spine ligaments. *J. Biomech. Eng.,* 122**,** 623-629.

Yoganandan, N., Nahum, A. M. & Melvin, J. W. 2014. *Accidental injury: biomechanics and prevention*, Springer.